Article

Cell

Excitable Dynamics and Yap-Dependent Mechanical Cues Drive the Segmentation Clock

Graphical Abstract

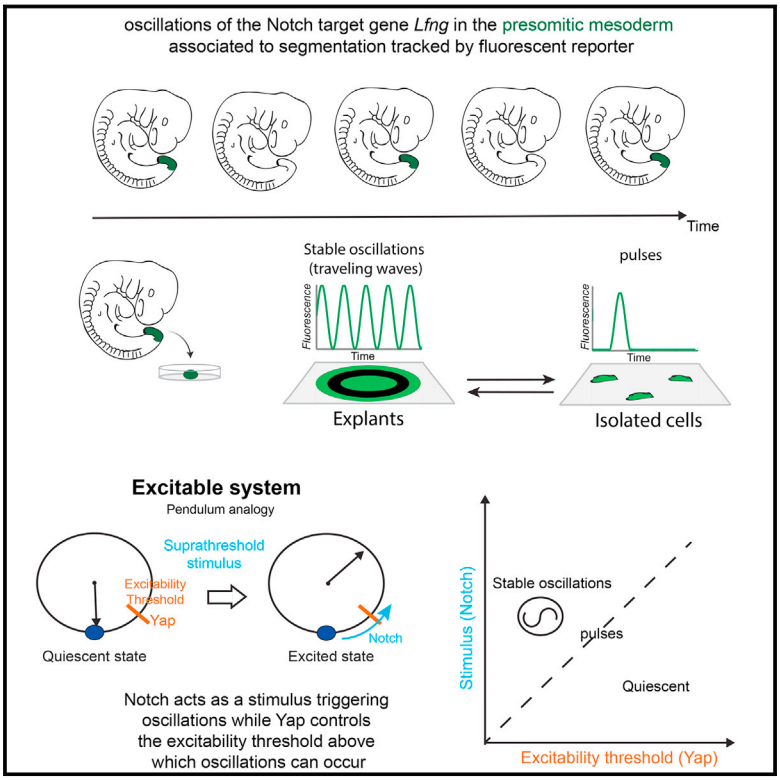

Highlights

- *In vitro* system supporting stable segmentation clock oscillations
- A cell-density effect controls the onset of oscillations *in vitro*
- Yap-dependent mechanical signal acts as a control parameter for oscillations
- Segmentation clock has properties of an excitable system

Authors

Alexis Hubaud, Ido Regev, L. Mahadevan, Olivier Pourquié

Correspondence

lmahadev@g.harvard.edu (L.M.), pourquie@hms.harvard.edu (O.P.)

In Brief

YAP and Notch collaborate to control collective cellular oscillations during somitogenesis.

Hubaud et al., 2017, Cell *171*, 1–15
October 19, 2017
http://dx.doi.org/10.1016/j.cell.2017.08.043

CellPress

Please cite this article in press as: Hubaud et al., Excitable Dynamics and Yap-Dependent Mechanical Cues Drive the Segmentation Clock, Cell (2017), http://dx.doi.org/10.1016/j.cell.2017.08.043

Article

Cell

Excitable Dynamics and Yap-Dependent Mechanical Cues Drive the Segmentation Clock

Alexis Hubaud,[1,2,7] Ido Regev,[3,8] L. Mahadevan,[3,4,5,*] and Olivier Pourquié[1,2,6,9,*]

[1]Institut de Génétique et de Biologie Moléculaire et Cellulaire (IGBMC), CNRS (UMR 7104), Inserm U964, Université de Strasbourg, Illkirch 67400, France

[2]Department of Genetics, Harvard Medical School and Department of Pathology, Brigham and Women's Hospital, 60 Fenwood Road, Boston, MA 02115, USA

[3]Paulson School of Engineering and Applied Sciences, Harvard University, Cambridge, MA 02138, USA

[4]Departments of Organismic and Evolutionary Biology and Physics, Harvard University, Cambridge, MA 02138, USA

[5]Wyss Institute for Biologically Inspired Engineering and Kavli Institute for Nanobio Science and Technology, Harvard University, Cambridge, MA 02138, USA

[6]Harvard Stem Cell Institute, Harvard University, Cambridge, MA 02138, USA

[7]Present address: Novartis Institute for BioMedical Research, Cambridge, MA 02139, USA

[8]Present address: Jacob Blaustein Institutes for Desert Research, Ben-Gurion University of the Negev, Sede Boqer Campus, Sede Boqer 84990, Israel

[9]Lead Contact

*Correspondence: lmahadev@g.harvard.edu (L.M.), pourquie@hms.harvard.edu (O.P.)

http://dx.doi.org/10.1016/j.cell.2017.08.043

SUMMARY

The periodic segmentation of the vertebrate body axis into somites, and later vertebrae, relies on a genetic oscillator (the segmentation clock) driving the rhythmic activity of signaling pathways in the presomitic mesoderm (PSM). To understand whether oscillations are an intrinsic property of individual cells or represent a population-level phenomenon, we established culture conditions for stable oscillations at the cellular level. This system was used to demonstrate that oscillations are a collective property of PSM cells that can be actively triggered *in vitro* by a dynamical quorum sensing signal involving Yap and Notch signaling. Manipulation of Yap-dependent mechanical cues is sufficient to predictably switch isolated PSM cells from a quiescent to an oscillatory state *in vitro*, a behavior reminiscent of excitability in other systems. Together, our work argues that the segmentation clock behaves as an excitable system, introducing a broader paradigm to study such dynamics in vertebrate morphogenesis.

INTRODUCTION

Molecular oscillators are involved in a wide range of biological processes, such as temporal ordering of cellular activities (cell cycle, circadian clock) or diversifying the coding repertoire of signaling pathways (nuclear factor κB [NF-κB], P53, and *Hes1* oscillations) (Levine et al., 2013; Sonnen and Aulehla, 2014). During development, the vertebrate presomitic mesoderm (PSM) experiences periodic traveling waves of cell signaling anticipating segment formation. This ''segmentation clock'' underlies the rhythmic segmentation of the precursors of the vertebrae and skeletal muscles in the paraxial mesoderm (Cooke and Zeeman, 1976; Hubaud and Pourquié, 2014; Oates et al., 2012; Palmeirim et al., 1997). These oscillations are associated with the cyclic activation of signaling pathways (Notch, Fgf, Wnt) and genes (*Hes/Her* transcription factors) in the PSM, which periodically instruct the formation of segments called somites. The cyclic activity of PSM cells relies on a complex genetic network composed of negative feedback loops with delay involving the Notch pathway and the transcriptional repressors of the Her/Hes family (Hubaud and Pourquié, 2014). The traveling waves arising from the coordinated oscillations of PSM cells progressively slow down and eventually stop as they move along posterior to anterior gradients of Fgf and Wnt signaling. These pathways control the competency of PSM cells to respond to the clock signal, which periodically triggers a genetic program leading to the individualization of segments (Aulehla et al., 2003; Dubrulle et al., 2001; Naiche et al., 2011; Sawada et al., 2001). At the individual cell level, previous theoretical studies have suggested that the PSM consists of a population of self-sustained cellular oscillators (Lewis, 2003; Morelli et al., 2009). In this scenario, cells are assumed to locally synchronize their phase with their neighbors through Notch signaling and to form waves traveling along the PSM (Oates et al., 2012).

Understanding the regulation and the dynamical properties of the segmentation clock has been difficult due to the lack of an appropriate *in vitro* system recapitulating this oscillatory behavior. The control of oscillations at the level of individual PSM cells has been experimentally studied in isolated cells *in vitro* (Masamizu et al., 2006; Webb et al., 2016). While dynamic pulses were reported, no stable oscillations were detected. Therefore, whether PSM cells harbor intrinsic oscillators or whether oscillations reflect an emergent property of the cell population could not be established. *In vitro* cultures of tail bud explants from the mouse reporter line *LuVeLu* (where the fluorescent protein Venus is driven by the promoter of the cyclic Notch target *Lunatic Fringe* [*Lfng*]) were shown to recapitulate oscillations of the segmentation clock in

two dimensions (Lauschke et al., 2013; Tsiairis and Aulehla, 2016). This system has allowed for the study of the collective behavior of cells and the generation of waves in the PSM (Lauschke et al., 2013). This experimental paradigm was also used to demonstrate the self-organizing properties of PSM cells that can reestablish wave-like pattern of activity upon dissociation and reaggregation (Tsiairis and Aulehla, 2016). In this set-up, however, oscillations are not stable as the explants cells differentiate and the period of oscillations progressively increases until it stops prior to segment formation as is observed *in vivo*.

Here, we report the establishment of a novel *in vitro* system, in which PSM cells from the *LuVeLu* reporter mouse maintain stable oscillations. Using this system, we examine the conditions required for the onset and the maintenance of *Lfng* oscillations in explants and single cells *in vitro*. We show that a quorum-sensing type of signal involving Notch and Yap signaling plays a critical role in controlling the onset and stability of oscillations. Our work shows that the segmentation clock exhibits properties of an excitable system with signatures of threshold for oscillations, pulsatile behavior, and the presence of a refractory period, behaviors that arise from the collective dynamics of the cell population.

RESULTS

PSM Cells Can Be Maintained in a Stable Oscillatory Regime *In Vitro*

To study the dynamics of the segmentation clock, we first established an *in vitro* system in which we can maintain PSM cells in a stable oscillatory state. For this purpose, we dissected and cultured explants of the posterior-most PSM from the tail bud of E9.5 embryos of the *LuVeLu* mouse reporter line (without ectodermal tissues) (Aulehla et al., 2008) (Figure 1A). When such PSM explants are cultured on fibronectin in a base medium-containing serum, they spread to form two-dimensional disk-like colonies of cells. Initially, these explants exhibit *LuVeLu* oscillations as they grow (from 0 to ~18 hr), but eventually the oscillatory domain shrinks reflecting the differentiation that starts at the periphery of the disk (from ~18 to 36 hr) (Figure 1B). These oscillatory dynamics are very similar to those reported in Lauschke et al. (2013) where similar explants (but containing ectoderm) are cultured in a minimal medium containing BSA. To maintain the explants in a stable oscillatory state, we added factors to the base medium to activate Fgf and Wnt pathways that are required to maintain cells in a cyclic, posterior PSM state *in vivo* (Aulehla et al., 2003; Dubrulle et al., 2001). Addition of the Wnt activator CHIR (CHIR99021) alone did not prevent the arrest of oscillations and differentiation, and oscillations were suppressed upon Fgf4 addition alone or in combination with CHIR (Figures 1B and S1A). Adding the BMP inhibitor LDN (LDN-193189), which is important for PSM specification *in vitro* (Chal et al., 2015), together with CHIR and FGF4 led to a significant upregulation of cyclic genes (Figure S1B) and to stable oscillations of the *LuVeLu* reporter (Figures S1A and S1B). Additionally, blocking the retinoic acid pathway and adding the ROCK inhibitor Y-27632 improved the cell viability and the stability of oscillations (Figure S1A).

With all the factors described above, we observed rhythmic concentric waves of the *LuVeLu* reporter with a period of 2.5 hr (152 ± 8 min) (Figure 1C; Movie S1), close to their reported periodicity *in vivo* (Lauschke et al., 2013). *In situ* hybridization for the cyclic gene *Hes7* indicated the existence of similar waves for this gene (Figure S1C). In mouse embryos, cells entering the posterior PSM express the markers *Tbx6* and *Msgn1* for around 12–18 hr and experience ~6 oscillations until they reach the anterior PSM, where they begin to differentiate (Aulehla et al., 2008; Nowotschin et al., 2012; Tam et al., 1982). In our conditions, explants maintained expression of posterior PSM markers such as TBX6, T, or *Msgn1* (Figure 1A), and segment boundary formation was not observed. Explants showed more than ~20 oscillations during a 48 hr culture period. No gradient of the Fgf targets phosphorylated ERK and *Spry2* was detected (n = 5/5, Figure 1D and n = 4/4, Figure S1D), suggesting that the explants do not display the spatiotemporal organization of the PSM. In contrast, the explants of Lauschke et al. (2013) recapitulate the PSM differentiation *in vitro.* These explants establish gradients of Fgf and Wnt signaling, along which *LuVeLu* oscillations progressively slow-down and arrest as in the embryo (Lauschke et al., 2013; Tsiairis and Aulehla, 2016). Together, this suggests that our culture conditions can block differentiation and maintain PSM cells in a stable oscillatory state.

Self-Organization of Oscillations and Waves in PSM Explants

We next examined the collective behavior of PSM cells in our system. Initially, all the cells in the PSM explant oscillate synchronously. As the explant spreads, a spatiotemporal pattern of traveling waves similar to a target pattern (i.e., a pattern of concentric waves emitted from a source) becomes established. No difference in the period of oscillations was found between the center and the periphery of the explants after their initial spreading (n = 33/33, Figure 2A). To probe whether these target waves are emitted by a special pacemaker population located at the center of the explant, we either removed this central region (Movie S2) or isolated it from the rest of the explant using laser or mechanical ablation. The remaining parts of the explants continued to display periodic traveling waves of the reporter (n = 4/4, Figure 2B), arguing for a kinematic nature of the wave.

We next dissociated explants from different embryos into single cells then mixed and re-aggregated the cells by centrifugation as described in Tsiairis and Aulehla, (2016). The aggregated explants recapitulated the organization of single tail bud explants, first exhibiting synchronized oscillations at the start of the experiment (2 hr after dissociation) (n = 15/15, Figure 2C; Movie S3) and then switching to traveling waves arranged in a target pattern (n = 7/15) with a similar period. Remarkably, the re-aggregated explants formed from the same preparation were observed to oscillate in synchrony, suggesting a quick phase-resetting leading to synchronized oscillations among cells originating from the different explants. Together, these data argue against the existence of a dedicated pacemaker that entrains other PSM cells and instead suggest that oscillations and traveling waves are an emergent property of the population of explant cells.

Evidence for Dynamical Quorum Sensing Controlling the Onset of Oscillations

To examine the *LuVeLu* dynamics at the level of isolated cells, we dissociated cells from the tail bud PSM and seeded them at

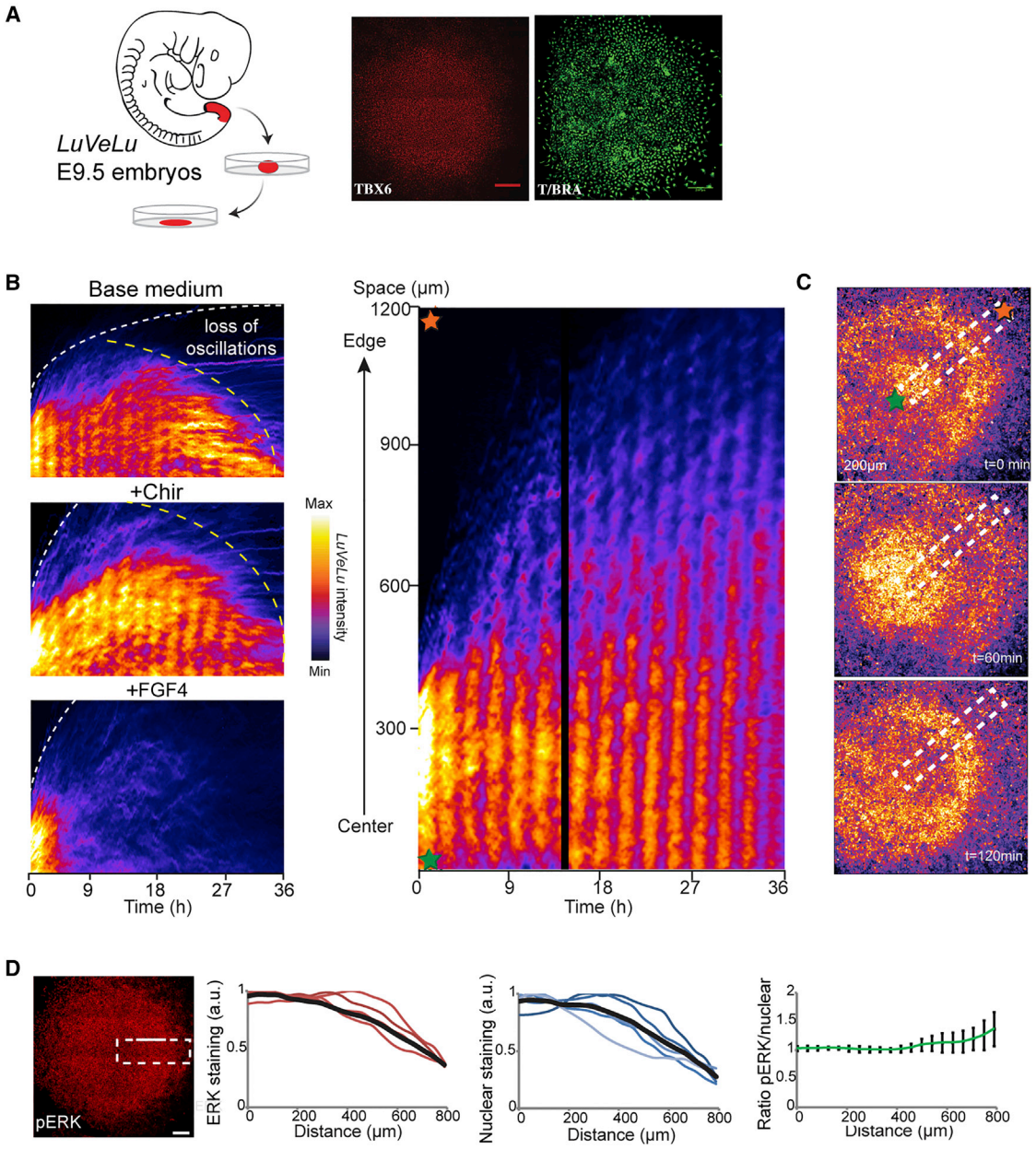

Figure 1. An *In Vitro* System to Study the Segmentation Clock

(A) Left: a mouse tail bud is dissected and plated on a fibronectin-coated dish. Right: after spreading, the tissue forms a monolayer of cells positive for the PSM markers TBX6 and T (after 1 day of culture: scale bar, 200 μm).

(B) Left: kymographs showing the *LuVeLu* fluorescence profile in a region from the center to the periphery of explants cultured in base medium, base medium plus Chir, and base medium plus FGF4. Right: kymograph showing the *LuVeLu* fluorescence profile along the dotted rectangle in (C) in conditions promoting stable oscillations (the discontinuity is due to a medium change).

(C) *LuVeLu* fluorescence intensity in an explant over a period of 120 min. Stars and dotted rectangle, region selected for the kymograph in (B).

(D) Left: immunostaining for pERK (scale bar, 200 μm). Middle: quantification of pERK staining (red) and nuclei staining (blue) from the center to the periphery of the explant in the dotted rectangle. The black line represents the average of the five explants. Right: ratio between pERK and nuclear staining (green ± SD) from the center to the periphery.

See also Figure S1 and Movie S1.

low-density on fibronectin-coated dishes in the same culture conditions as the explants. No sustained oscillations were detected in these cultures, although we observed aperiodic pulses of reporter activation, usually preceding cell division (n = 5/5, Figure 3A). The reporter was progressively extinguished during an overnight culture (Movie S4) even though most cells retained

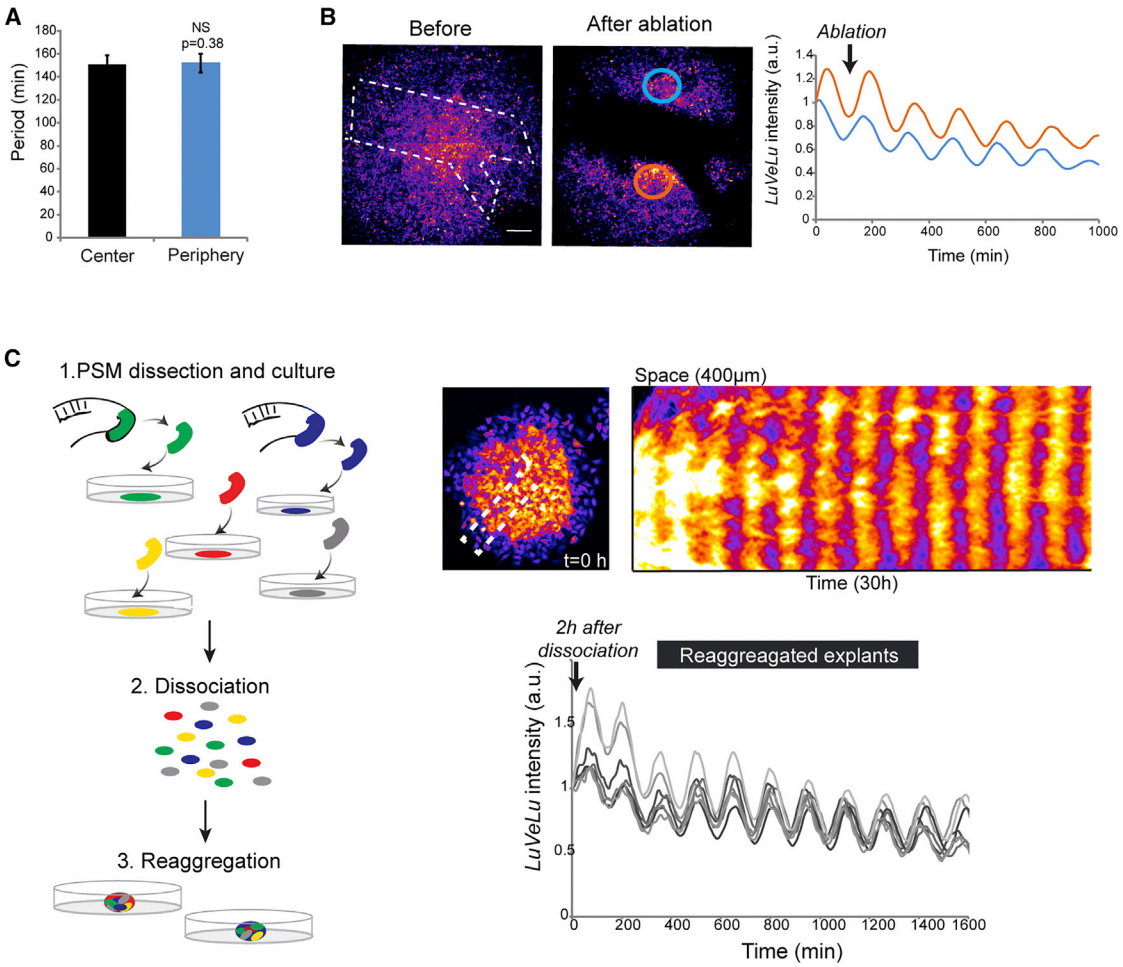

Figure 2. Self-Organization of Oscillations and Waves

(A) Period (± SD) of *LuVeLu* oscillations in the center and periphery of explants (4 explants, n = 33, t test p = 0.38).

(B) Left: explant before and after mechanical ablation to remove the center of oscillations. Right: *LuVeLu* fluorescence intensity over time for two regions of the cut explant (blue and orange circles).

(C) Left: several explants (n = 11) are dissociated, and single cells are then mixed and reaggregated as explants (n = 7). Top right: snapshot of a reaggregated explant and associated kymograph. Bottom right: *LuVeLu* fluorescence intensity over time for reaggregates (2 hr after the dissociation).

See also Movies S2 and S3.

expression of the posterior PSM marker TBX6, suggesting that they conserve their PSM identity (n = 101/147, Figure 3A). Re-aggregating isolated cells that stopped oscillating after an overnight culture led to the re-initiation of collective oscillations and traveling waves in the re-aggregated explants (Figure 3A). Thus, dissociated cells cultured in these conditions are in a quiescent (non-oscillatory) yet competent state and maintain their PSM identity independently of their oscillatory state.

To better quantify this effect, we used circular fibronectin micropatterns of defined size (80 µm in diameter), seeded with different densities of dissociated cells. At full confluency, cells on the micropatterns display synchronous oscillations (Figure 3B), while no oscillations are observed at low cell density (n_{low} = 12/12, Figure 3B). As the number of starting cells increased on the micropatterns, a dose-dependent rescue of the oscillations was observed (n_{inter} = 4/5, Figure 3B; n_{high} = 5/5, Movie S5). This demonstrates a density-dependent effect on the control of onset of *LuVeLu* oscillations.

Notch Signaling Is Necessary for *LuVeLu* Oscillations

A natural candidate for regulating this density-dependent effect is Notch signaling, as the pathway activation requires cell-cell contacts to trigger the response of membrane-bound receptors and ligands. Treatment with γ-secretase inhibitors (DAPT or LY-411575) that inhibit Notch signaling blocked oscillations on the micropatterns leading to damped oscillations at the collective level (Figures 4A and S2A; Movie S6, n = 3/3-LY-411575; n = 4/4-DAPT). Similarly, *Hes7* was barely detected by *in situ* hybridization after treatment with DAPT (Figure S2B), and qPCR analysis of *Lfng* and *Hes7* confirmed that they are strongly downregulated (~3-fold) (Figures S2C and S2D), indicating that Notch signaling is effectively blocked by DAPT. To follow the

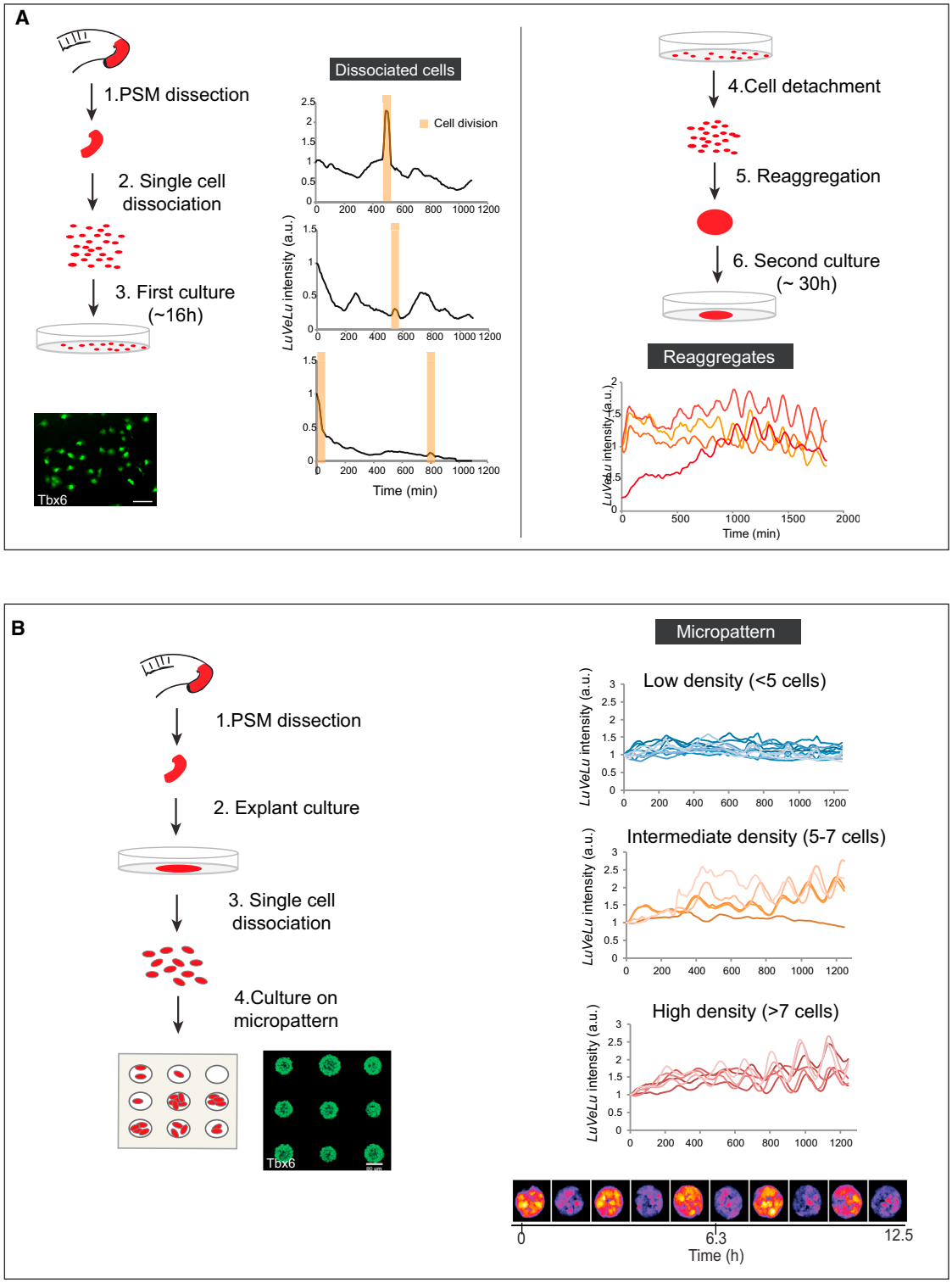

Figure 3. A Quorum-Sensing Effect Controls the Onset of Oscillations

(A) Top left: explants are dissociated and single cells are seeded on a dish coated with fibronectin. Graphs showing the *LuVeLu* fluorescence intensity over time for three representative cells. Orange windows: cell divisions. Bottom left: immunostaining for TBX6 in dissociated cells after an overnight culture (scale bar, 100 μm). Top right: after an overnight culture, cells are detached and reaggregated to form an explant. Bottom right: *LuVeLu* fluorescence intensity over time for aggregates from isolated cells cultured overnight (right, n = 4). Each line corresponds to one aggregate.

(legend continued on next page)

response of individual cells to Notch inhibition, we infected *LuVeLu* explants with a low-titer lentivirus expressing mCherry to label isolated cells, and we quantified *LuVeLu* fluorescence in these cells. All individual cells examined showed a dampening of oscillations after addition of the γ-secretase inhibitor (~2-fold, n = 8/8) (Figures 4B and S2D). The strong decrease in the amplitude of oscillations both at the individual and collective level indicates that the cells enter a quiescent state that must be contrasted with a transition involving only desynchronization (Figure 4C). Thus, in our explant cultures, Notch activation is necessary for normal *LuVeLu* oscillations.

We next tested whether Notch activation is sufficient to restore *LuVeLu* oscillations in isolated PSM cells. Dissociated PSM cells cultured on fibronectin stop oscillating and show strongly decreased expression levels of the Notch targets *Lfng* and *Nrarp* (Figure 5A). To activate Notch signaling in dissociated cells, we coated plates with fibronectin and the Notch ligand Delta-like 1 (DLL1) prior to seeding PSM cells. In these conditions, DLL1 is sufficient to activate an artificial Notch reporter in CHO cells (Figures 4D, 4E, and S2E) (Sprinzak et al., 2010). Culturing dissociated PSM cells onto plates coated with DLL1 induced the expression of *Lfng* and *Nrarp* to a level similar to that observed in explants but was not sufficient to induce *LuVeLu* oscillations (Figure 4F). Thus, Notch activation alone is not sufficient to restore oscillations in single cells cultured in these conditions, suggesting the existence of a second factor involved in the dynamical quorum sensing.

Mechanical Cues and Yap Signaling Control the Oscillatory Transition

Surprisingly, we found that the substrate itself had an effect on the oscillatory state of isolated PSM cells. Substituting fibronectin by BSA as a coating substrate was enough to restore sustained oscillations in single cells even in the absence of DLL1 (with a period close to the explant period: 175 ± 22 min) (Figures 4F and 4G; Movie S7). Dissociated PSM cells cultured on fibronectin and on BSA exhibit strikingly different morphologies and behavior, with the former being elongated and highly motile while the latter are roundish and mostly static (Movies S4 and S7). These experiments suggest that cell-substrate adhesion can control the oscillatory state of isolated PSM cells.

Differences in cell-shape linked to cytoskeletal organization and to adhesion substrates such as fibronectin have been reported to modulate Yap signaling (Dupont, 2015; Dupont et al., 2011; Kim and Gumbiner, 2015). Culturing dissociated cells on fibronectin was associated with a strong activation of the Yap pathway targets *ANKRD1* and *Cyr61* compared to culturing on a BSA substrate (Figure 5A). In parallel, culture of dissociated cells on BSA led to a significant upregulation of targets of the Fgf and Wnt pathways compared to cultures on fibronectin (Figure 5A). Furthermore, when cells were cultured on fibronectin, we observed a preferential nuclear localization of YAP1, indicative of an activation of the Yap pathway (n = 128/169) (Figures 5B and S3A). By contrast, YAP1 was localized both in the nucleus and cytoplasm in the same cells cultured on BSA (n = 97/129) (Figure S3A). Therefore, this argues that adhesion to fibronectin can activate Yap signaling in dissociated cells.

These observations further suggest that Yap activation inhibits oscillations in single cells cultured on fibronectin. To test this, we treated isolated cells cultured on fibronectin with latrunculin A (LatA), an inhibitor of actin polymerization, known to repress Yap signaling (Dupont et al., 2011; Zhao et al., 2012). As expected, treating dissociated cells cultured on fibronectin with LatA led to a downregulation of *Ankrd1*, *Cyr61*, and *Ctgf* (Figure 5A). Remarkably, in these conditions, single cells displayed *LuVeLu* oscillations with a period similar to that observed in explants (162 ± 8 min) (Figures 5C and S4; Movie S8). To further link the effect of LatA to Yap signaling, we infected dissociated PSM cells with a lentiviral construct expressing a constitutively active form of YAP1 (YAPS5A) (Dupont et al., 2011). When these cells were treated with LatA, no *LuVeLu* oscillations were observed in infected cells (n = 22/23, Figure 5D). In contrast, oscillations were detected in cells infected with a control construct (n = 17/19, Figure 5D). The effect of LatA is independent of Notch cleavage by the γ-secretase complex, as oscillations were observed in single cells treated with LatA and DAPT (Figure 5C). Furthermore, LatA treatment alone was unable to activate an artificial Notch reporter in CHO cells (Figure S2E) (Sprinzak et al., 2010). Surprisingly, this indicates that, in this context, *LuVeLu* oscillations do not depend only on Notch signaling but that other signal inputs are involved.

In tail bud explants that are also cultured on fibronectin, Yap targets were downregulated compared to isolated cells in similar conditions, and YAP1 was found both in the nucleus and cytoplasm like in the posterior PSM in mouse embryos (Figure 5B). A similar pattern was observed for phospho-YAP1 distribution analyzed with an antibody recognizing the Ser127 phosphorylated form of YAP1 (data not shown). Thus, increasing cell density can overcome the effect of fibronectin on Yap activation. Accordingly, in micropatterns seeded with different cell densities, we found an inverse correlation between the nucleocytoplasmic ratio of YAP1 and cell density (Figures S3B) (r^2 = 0.15, p value = 0.005). Hence, Yap signaling is regulated by cell density, as demonstrated in other systems. Explants cultured on fibronectin in presence of LatA continued to display traveling waves despite cells becoming roundish and static as observed with isolated cells (n = 4/4, Movie S9). Blocking Notch with DAPT in these LatA-treated explants disrupts collective oscillations and waves (n = 4/4, Movie S9). However, at the individual level, we observed that neighboring cells treated with LatA and DAPT harbored desynchronized oscillations, supporting a role for Notch only in the synchronization of oscillations in this context (Figure 5E).

(B) Top left: explants are dissociated, cultured overnight, then dissociated in single cells and seeded on fibronectin micropatterns. Bottom left: TBX6 immunostaining on cells seeded at high density on micropatterns after overnight culture (scale bar, 80 μm). Top right: *LuVeLu* fluorescence intensity over time for micropatterns with various initial cell numbers (each line corresponds to one micropattern). Bottom right: *LuVeLu* fluorescence intensity for cells seeded at high density on a fibronectin micropattern.
See also Movies S4 and S5.

Please cite this article in press as: Hubaud et al., Excitable Dynamics and Yap-Dependent Mechanical Cues Drive the Segmentation Clock, Cell (2017), http://dx.doi.org/10.1016/j.cell.2017.08.043

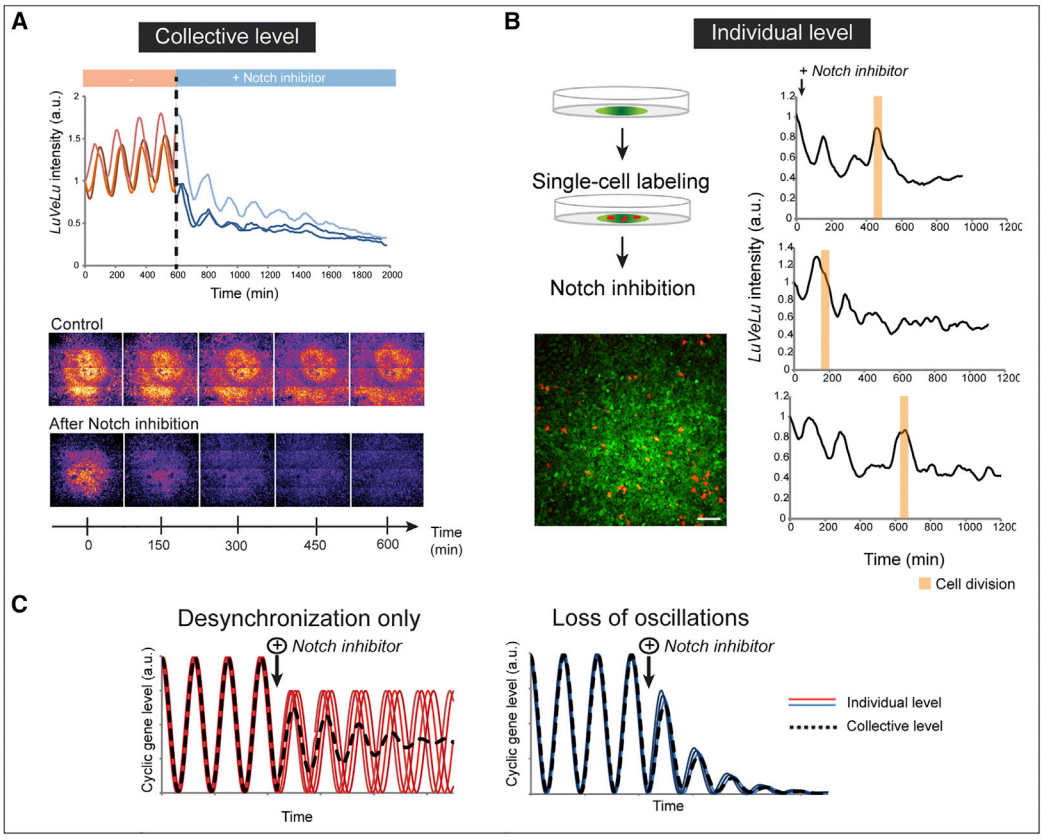

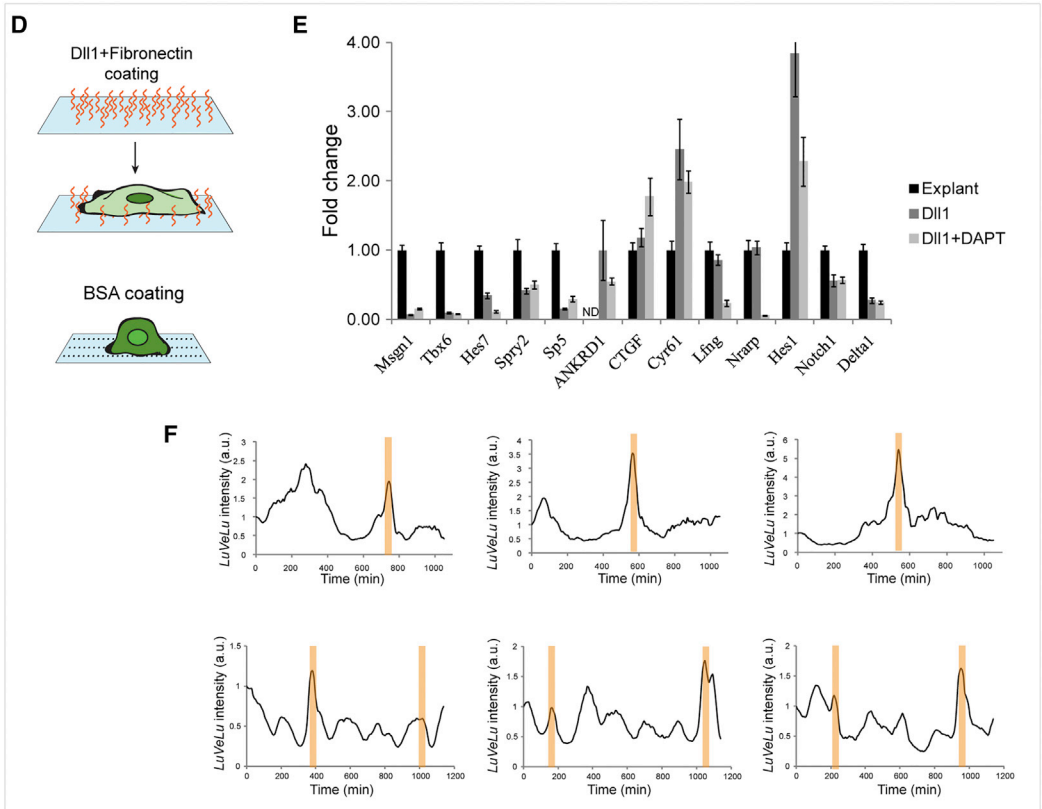

(legend on next page)

To validate the effect of Yap signaling *in vivo*, we electroporated the YAPS5A constitutively active form of YAP1 in the PSM of chicken embryos downstream of a tetracycline-inducible promoter. Oscillations of the segmentation clock were examined by *in situ* hybridization for the cyclic gene *LFNG*. In electroporated embryos treated with doxycycline, we observed an upregulation of *LFNG* in the PSM and a disruption of cyclic activity evidenced by the uniform expression pattern observed in most of the embryos (n = 16/20, Figure 5F). In contrast, embryos electroporated with the construct without doxycycline displayed the normal pattern of *LFNG* with the characteristic three phases of expression (n = 17/19, Figure 5F) (Pourquié and Tam, 2001).

Together, this shows that the quorum sensing signal controlling the onset of oscillations involves inhibition of Yap signaling in parallel to Notch activation.

Excitability as a General Framework for *LuVeLu* Oscillations

Current models of the segmentation clock cannot explain our observation that isolated PSM cells can be switched from a quiescent state to an oscillatory state. This dynamic behavior could be explained if the segmentation clock behaves as an excitable system, in a manner that is qualitatively similar to other known biological excitable systems such as neurons or social amoebae (Winfree, 2001). Excitability in these dynamical systems is characterized by a few common properties (Izhikevich, 2000; Murray, 2011; Winfree, 2001), notably: (1) the presence of a threshold that separates a quiescent state from an excited state (large-amplitude oscillations), (2) a large response to a strong stimulation associated with a refractory period, and (3) in spatial settings, a complex self-organization, characterized by traveling waves (Figure 6A). Importantly, excitable systems can undergo a sharp transition to synchronized oscillations as individual cells simultaneously cross a critical signal level corresponding to the excitability threshold (quorum sensing).

To probe these conceptually different paradigms, we examined how cells can transition from a non-oscillatory to an oscillatory state. Treating PSM cells seeded at high-density on fibronectin micropatterns with the Notch inhibitor DAPT for 6 hr arrests the collective oscillations (Figure 6B). When the treated cells are transferred back to control medium, we observed an immediate recovery of the *LuVeLu* oscillations (Figure 6B, n = 12/12) as expected for an excitable system (Kamino et al., 2011). In contrast, if Notch was only required for the synchronization, the amplitude of collective oscillations would progressively increase, as individual oscillators coordinate their cycling (Figures 6B and S2D). Together, this suggests that in this context, Notch signaling acts as a component of the signal triggering excitability.

The existence of a refractory period following stimulation is another important characteristic of excitable systems. A testable prediction of the existence of a refractory period is that colliding traveling waves will annihilate each other (Argentina et al., 1997). To test this experimentally, we cultured pairs of explants contacting each other and arranged so that the waves generated by the two explants would eventually meet along the contact area as the explants spread out. We see that the traveling waves from one explant do not propagate into the other explant and are annihilated on collision for both in-phase or anti-phase explants (Figure 6C; Movie S10; data not shown, n = 6/10). We also observed situations, in which one target pattern invades into the neighboring explant while the other disappears (data not shown, n = 3/10). These properties of wave propagation and annihilation are thus consistent with the existence of a refractory period characteristic of excitable systems. Together, our observations suggest that the oscillator controlling *LuVeLu* oscillations in the PSM behaves as an excitable system.

An Excitable Model Captures the *LuVeLu* Dynamics In Silico

To further validate this theoretical framework, we tested whether a general mathematical model of excitability can account for our data and predict novel experimental results. For this, we used the FitzHugh-Nagumo model (Figure 7A) (Fitzhugh, 1961; Nagumo et al., 1962) that consists of a fast activator and a slow repressor interacting together. It has been used to describe the behavior of excitable systems such as neurons and serves to recapitulate the essential features of excitable behavior, independent of the actual molecular details of the system (Mehta and Gregor, 2010; Sgro et al., 2015; Winfree, 2001). In our system, we assume that Yap-dependent mechanical cues (cell adhesion, actin cytoskeleton organization) modulate the excitability threshold, while Notch signaling is conceived as an external inducer for the activator (equivalent to the applied current for neurons).

Our simulations show that when the Notch stimulus is strong enough, the system can cross the Yap-dependent excitability threshold leading to self-sustained limit cycle oscillations (Figure 7B). Such a situation is predicted in tail bud explants and in the PSM of the embryo where Notch is active and Yap is activated at an intermediate level. In isolated cells cultured on fibronectin, the loss of the density-dependent signal leads to strong Yap activation raising the threshold for oscillations

Figure 4. Notch Signaling Is Required for the Clock Oscillations

(A) Top: *LuVeLu* fluorescence intensity for 4 explants over time, first without Notch inhibitor (LY-411575) (red), then after its addition (blue). Bottom: snapshots showing fluorescence intensity for a control and a DAPT-treated explant every 150 min.

(B) Left: *LuVeLu* explants were infected with a lentiviral construct to mark cells with mCherry (scale bar, 200 μm), then a Notch inhibitor was added to the culture. Right: *LuVeLu* fluorescence intensity over time for three cells right after the addition of Notch inhibitor. Orange windows, cell divisions.

(C) Distinct behaviors at the individual and collective level in the case of desynchronization (left) and loss of oscillations (right).

(D) Scheme illustrating the experimental protocol (fibronectin was omitted on the scheme) for DLL1 (top) or BSA coating (bottom).

(E) qPCR analysis showing fold change in gene expression (± SD) for dissociated cells cultured overnight on fibronectin plates coated with DLL1 with and without DAPT (20 μM). Normalization was performed with the DLL1 sample. ND, non-detected.

(F) *LuVeLu* fluorescence intensity over time for dissociated cells cultured on DLL1-coated (top) and on BSA-coated substrate (bottom). Orange boxes, cell divisions.

See also Figure S2 and Movie S6.

Please cite this article in press as: Hubaud et al., Excitable Dynamics and Yap-Dependent Mechanical Cues Drive the Segmentation Clock, Cell (2017), http://dx.doi.org/10.1016/j.cell.2017.08.043

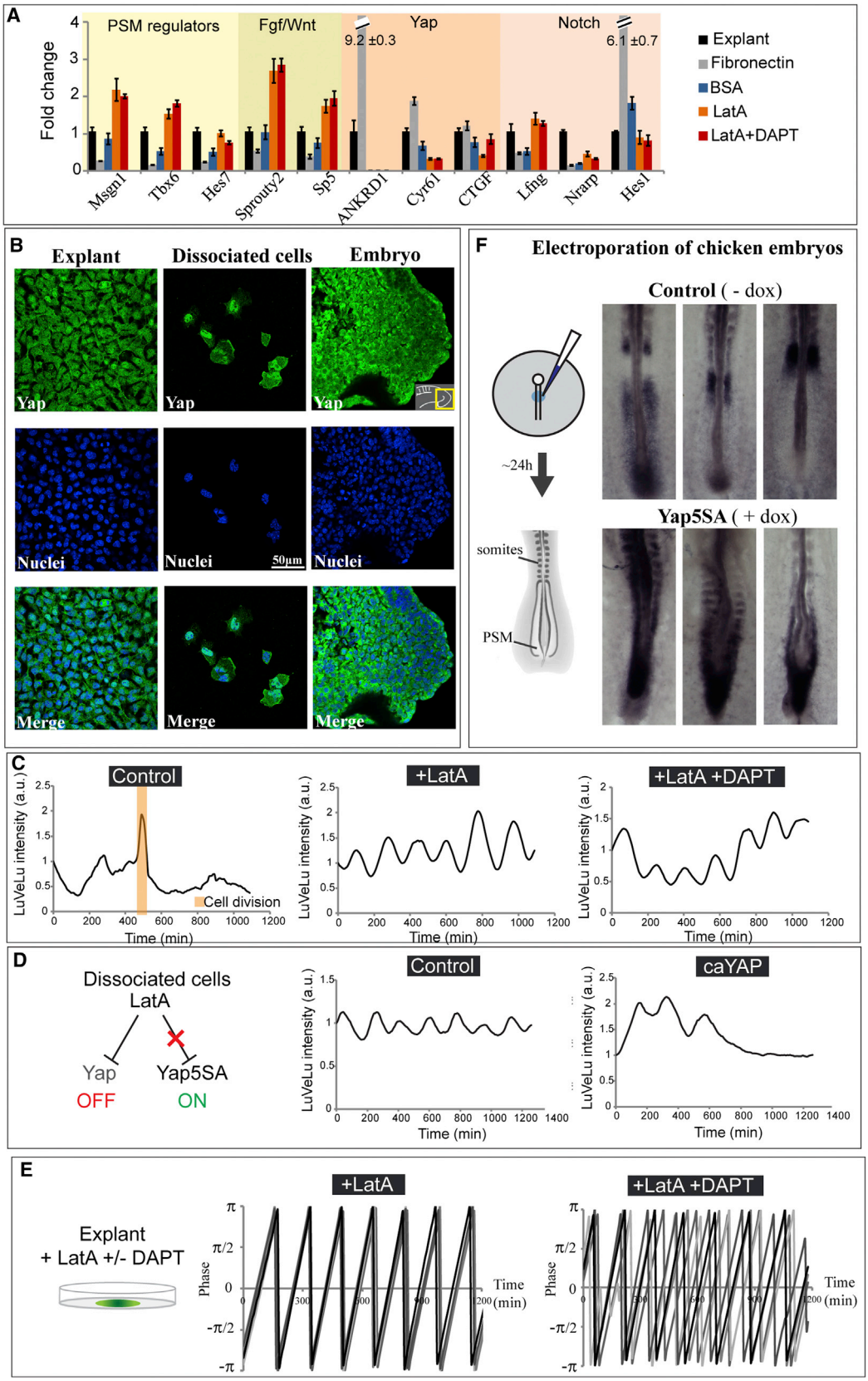

(legend on next page)

(Figure 7C). Together with the downregulation of Notch signaling, this prevents isolated cells from crossing the excitability threshold and thus oscillations are arrested with cells remaining in a quiescent state that is reversible (Figure 7C). This model also accurately predicts the results of Notch inhibition or Notch rescue experiments described in Figures 4A, 4B, 6B, and S2 (Figures 7D and 7E). A prediction of our mathematical model is that experimentally raising the excitability threshold by activating Yap should suppress oscillations in explants despite the presence of a Notch stimulus (Figure 7G). Such a situation is observed when infecting tail bud explants with a lentivirus expressing a constitutive active form of YAP1 (YAP5SA) (Figures 7H and 7I). In this context, *LuVeLu* oscillations are damped, consistent with an increase in the excitability threshold (Figure 7G). This model also explains why restoring Notch activation to endogenous levels by culturing isolated cells on the DLL1 ligand and fibronectin is not sufficient to trigger oscillations, as this leads to strong Yap activation triggered by the fibronectin substrate.

Conversely, the model predicts that reducing Yap signaling by culturing cells on a BSA substrate, by LatA treatment or by increasing cell density, should lower the excitability threshold resulting in an easier trigger of oscillations. This could explain why oscillations are observed even in the absence of the Notch stimulus in isolated cells treated with LatA. Our interpretation is that in such a case, due to the very low excitability threshold, noise or fluctuations in gene expression may be sufficient to trigger the oscillatory behavior (Figure 7F). Also, treating tail bud explants with LatA is expected to downregulate Yap signaling and thus to decrease the excitability threshold. Therefore, no effect on the oscillations is expected, a situation that is verified *in vitro* despite the striking effect on cell morphology and behavior (Movie S9).

A more quantitative prediction borne out by the model is that as the excitability threshold is lowered, the frequency of pulses will increase (Figures 7J and 7K). To test this, we treated dissociated cells on fibronectin with increasing doses of LatA and counted the frequency of *LuVeLu* pulses during the experiment. We see that the frequency indeed increases with the dose of LatA (Figures 7J–7M), as predicted by the simulations.

Thus, our excitable model, in which we hypothesize that Notch signaling provides a stimulus to trigger oscillations while Yap signaling controls the excitability threshold, can accurately predict and explain experimental results including counterintuitive ones.

DISCUSSION

Our work leads to three major insights into the regulation of the segmentation clock. First, using an *in vitro* system in which stable oscillations of the segmentation clock can be maintained in PSM explants and in isolated cells, we identify a novel type of regulatory input in the mouse segmentation clock that involves cell-matrix interaction and cytoskeleton organization via the Yap pathway. Second, we demonstrate that PSM cells can exist in a quiescent state and can be switched to an oscillatory state in response to a cell density-dependent signal involving Notch and Yap signaling. Third, we show that our experimental observations on the generation of oscillations are best explained in the context of an excitable oscillator model, which goes beyond previously postulated coupled-phase oscillators and serves as a more general model of the segmentation clock.

We report the establishment of a culture system of tail bud explants of the *LuVeLu* reporter mouse, which can be maintained in a stable oscillatory state. This system demonstrates strikingly different dynamic behaviors compared to the *in vitro* culture system recapitulating oscillations described in Lauschke et al., (2013) and Tsiairis and Aulehla (2016). The major difference between the two systems is the culture medium, which in our case, includes Fgf/Wnt activators and a BMP inhibitor. These pathways are known to crosstalk with Yap signaling, potentially leading to a different regulation of the excitability threshold in the two conditions (Hansen et al., 2015). Another difference is the presence of serum in our culture medium. Oscillations of the cyclic gene *Hes1* with a 2-hr period can be triggered with a serum shock in fibroblasts (Hirata et al., 2002), suggesting that serum might also play a role in the regulation of oscillations. Interestingly, periodic regulation of MRTF by actin polymerization downstream of a circulating circadian signal present in serum leads to periodic oscillation of transcription controlled by SRF (Gerber et al., 2013). Whether periodic actin polymerization takes place in the PSM is an interesting possibility that remains to be investigated. Oscillations of the Yap target *Cyr61* have been reported in the mouse PSM suggesting that the Yap pathway could also be regulated in a periodic fashion (Dequéant et al., 2008).

In zebrafish, Notch signaling has been proposed to play a role essentially restricted to the synchronization of oscillations (Oates et al., 2012). In mouse somitogenesis, the role of Notch signaling has been controversial: while blocking the pathway in embryos leads to the disappearance of *Lfng* oscillations (Barrantes

Figure 5. Mechanical Factors and Yap Signaling Control the Oscillatory Dynamics

(A) Expression profiles of PSM markers and signaling pathways targets for explants, and isolated cells cultured on fibronectin or BSA, with and without inhibitors (LatA, DAPT). Fold changes compared to the explant level are represented (± SD).

(B) Immunostaining of YAP1 in explant (left), in isolated cells (middle) cultured on a substrate coated with fibronectin or in the posterior PSM of E9.5 mouse embryo (right).

(C) *LuVeLu* fluorescence intensity over time for three dissociated cells on fibronectin (left), on fibronectin with LatA (middle), or on fibronectin with LatA and the Notch inhibitor DAPT (right). The graphs are representative of the behavior of >5 cells.

(D) Left: LatA inhibits the Yap pathway, while expression of a constitutively active form of YAP1 (YAP5SA) forces its activation in presence of the drug. Right: *LuVeLu* fluorescence intensity over time for two representative dissociated cells treated with LatA and infected with a constitutive active form of YAP1 (YAP5SA) (right) or a control vector (left). Graphs are representative of the behavior of >5 cells.

(E) Phase of the *LuVeLu* oscillations in neighboring cells of explants treated with LatA (left) or both LatA and DAPT (right).

(F) Left: chicken embryos were electroporated at the streak stage with an inducible vector expressing a constitutive active form of YAP1 (YAP5SA). Right: *in situ* hybridization for the cyclic gene *LFNG* in electroporated embryos treated without (top) or with (bottom) doxycycline.

See also Figures S3 and S4, Table S1, and Movies S7, S8, and S9.

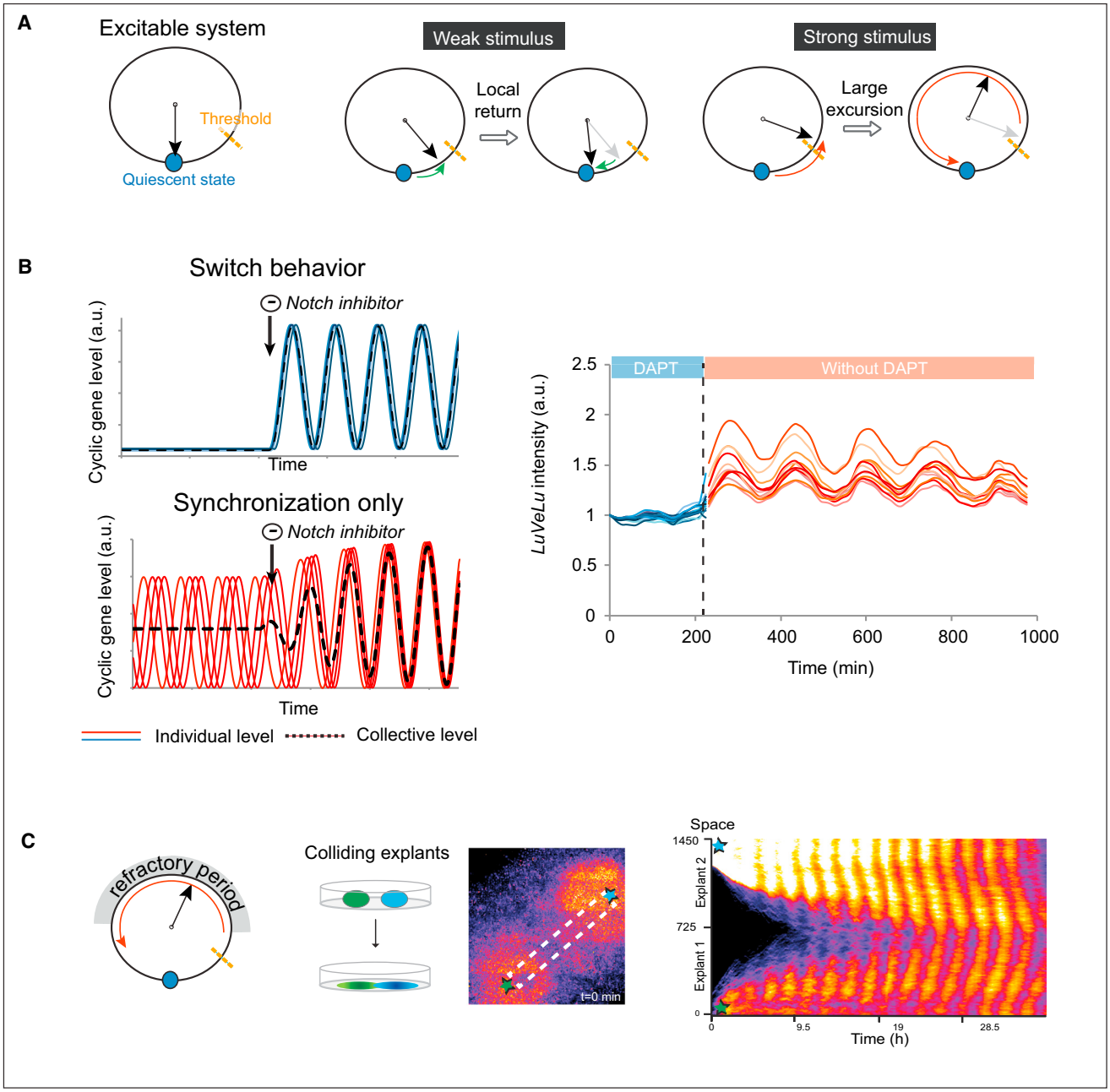

Figure 6. Excitable Properties of the *LuVeLu* Oscillations

(A) Graphical representation of an excitable system. Left: an excitable system can be in a quiescent state. After a weak stimulus (middle), the system locally comes back to its initial state. If the stimulus crosses the excitability threshold (right), the system does a large excursion (pulse) before returning to its initial state.

(B) Left: distinct behaviors at the individual and collective level showing exit from quiescence of an excitable system (top) and in case of resynchronization (bottom). Right: *LuVeLu* fluorescence intensity in micropatterns over time, in the presence of Notch inhibitor (blue) and after its removal (red).

(C) Left: scheme showing the existence of a refractory period after the excitation of the system. Middle: experimental procedure and snapshot of a collision of two explants. Stars and dotted rectangle, region selected for the kymograph. Right: kymograph associated with the white rectangle.

See also Movie S10.

et al., 1999; Ferjentsik et al., 2009), other studies reported that oscillations are maintained, but desynchronized, when Notch is inhibited (Okubo et al., 2012; Tsiairis and Aulehla, 2016). Notch1 and DLL1 oscillations could underlie the pulse dynamics (Bone et al., 2014; Kim et al., 2011; Liao et al., 2016; Shimojo and Kageyama, 2016). However, restoration of non-oscillatory expression of DLL1 in the mouse PSM leads to the formation of normal somites (Preuße et al., 2015). Our data suggest that

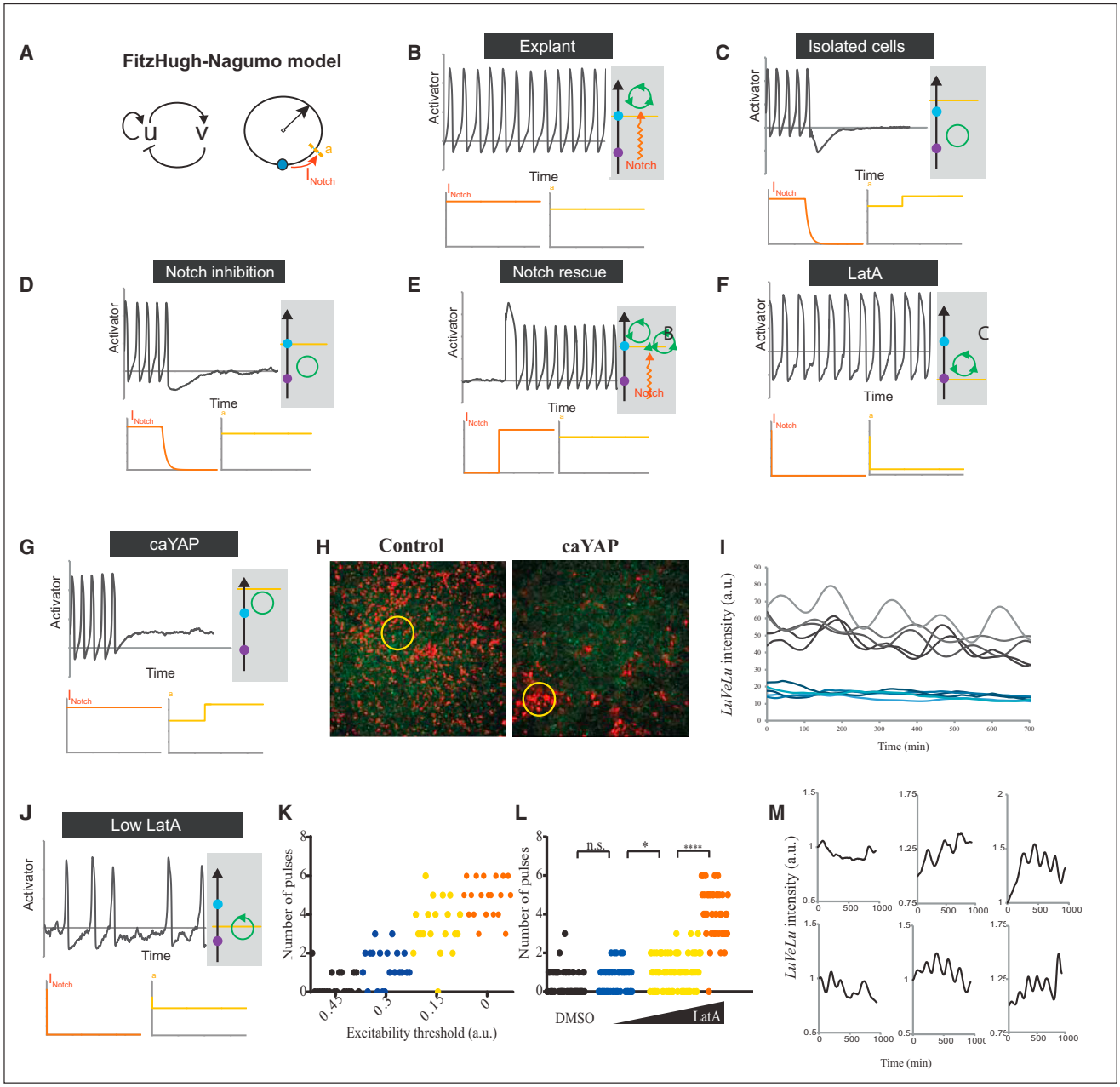

Figure 7. Simulations Using the FitzHugh-Nagumo Model Predict Experimental Results

(A) FitzHugh-Nagumo model with an activator (u) and a repressor (v). In the simulations, the Yap pathway acts on the excitability threshold (a), while Notch is modeled as an external current (I_{Notch}).

(B–F) Simulations of different experimental conditions. (B) Explant cell. (C) Isolated cell on fibronectin. (D) Explant cell treated with DAPT. (E) Explant cell treated with DAPT, then switched to control medium. (F) Isolated cell on fibronectin treated with LatA.

(G) Activator dynamics over time after elevation of the excitability threshold.

(H) *LuVeLu* explants infected with either a control lentivirus or a lentivirus expressing a constitutive active form of YAP1; infected cells are positive for mCherry (red).

(I) *LuVeLu* fluorescence intensity over time in a region of interest (yellow circles) infected with a control (black) or caYAP-expressing (blue) lentivirus.

(J) Activator dynamics over time when I_{Notch} levels are close to the excitability threshold.

(K) number of activator pulses in simulations of the FitzHugh-Nagumo model with various excitability thresholds.

(L) Number of *LuVeLu* pulses over the duration of the experiment (22 hr) for isolated cells treated with different doses of LatA.

(M) *LuVeLu* fluorescence intensity over time for isolated cells treated with the same suboptimal dose of LatA (0.3 μM).

in the excitable regime, Notch signaling is required both for the initiation (i.e., to cross the excitability threshold) and for the synchronization of oscillations. In the self-oscillatory regime (i.e., when the system is above the excitability threshold as when lowering Yap signaling for instance), Notch signaling would only be needed to synchronize oscillators. These effects might result in part from Yap interacting with Notch signaling as demonstrated in other systems (Manderfield et al., 2015; Totaro et al., 2017). Because the cyclic activity induced by LatA treatment was observed independently of γ-secretase activity, it raises the question of the pacemaker controlling *Lfng* oscillations, as this gene is considered a direct Notch target (Morales et al., 2002). The Hes7 transcriptional repressor might be implicated in this dynamic regulation of *Lfng*. Hes7 is involved in a negative feedback loop with delay that plays a central role in triggering oscillations of the mouse segmentation clock by repressing its own expression as well as that of *Lfng* (Kageyama et al., 2007). In our explants, *Hes7* is downstream of Notch signaling as its expression is downregulated by DAPT, but like *Lfng*, its expression is rescued by treatment with LatA (even in presence of DAPT). These findings suggest that other inputs converge to the oscillatory regulation of *Hes7* and *Lfng* in parallel to Notch. Fgf signaling that controls *Hes7* oscillations in the posterior PSM is an example of such a parallel input (Niwa et al., 2007).

We show that culture on a BSA substrate or interfering with the actin cytoskeleton contractility with LatA is sufficient to rescue oscillations at the single-cell level. Because we observed a decrease in Yap signaling with LatA, and because expression of a constitutive active form of YAP1 was able to block oscillations in drug-treated cells, we linked this mechanical effect to the Yap pathway. *Yap1*$^{-/-}$ mouse mutants exhibit a truncated axis but they form anterior somites (Morin-Kensicki et al., 2006). In *Xenopus* and fish, Yap loss-of-function alters embryos gastrulation and elongation but does not block somitogenesis (Gee et al., 2011; Hu et al., 2013; Porazinski et al., 2015). Yap is often shown to signal together with the related Taz/Wwtr1 protein. However, in contrast to *Yap* null mutants that show a strong phenotype early in development, mouse null mutants for Taz/Wvtr1 are viable and do not show segmentation defects (Hossain et al., 2007). Biomechanical changes during PSM development could act on the segmentation clock via the Yap pathway and thus couple patterning and morphogenetic events such as gastrulation or epithelialization of the PSM. However, no obvious correlation between the nucleo-cytoplasmic localization of YAP1 and the onset or arrest of oscillations in the mouse PSM could be observed (data not shown). Our results suggest that mechanical cues are critical for controlling the dynamics of the *LuVeLu* reporter pointing to a potential regulatory mechanism of the segmentation clock by morphogenetic events.

Furthermore, we show that adhesion to fibronectin leads to PSM cells spreading and Yap activation, inhibiting oscillations in dissociated cells *in vitro*. Remarkably, in the chicken PSM, fibronectin presents an antero-posterior gradient suggesting that it might play an inhibitory role on oscillations *in vivo* (Duband et al., 1987; Ostrovsky et al., 1983). Webb et al. (2014) also noted a correlation between cell spreading and the absence of oscillations of a Her1-YFP reporter in dissociated zebrafish PSM cells. Assuming a variation in the excitability threshold caused by a change in the mechanical response of the cells could explain this behavior. Together, our observations also show that mechanical conditions *in vitro* can strongly affect cell signaling prompting us to be cautious while using *in vitro* models.

Excitable properties of the signaling circuit could impact the onset of the segmentation clock as cells enter the PSM. Indeed, previous work in zebrafish has shown that PSM progenitors first do not oscillate, but express low and steady levels of cyclic genes (Mara and Holley, 2007). As they move in the PSM and mix with other cycling neighbors, cells start oscillating in a DeltaD-dependent manner. This is consistent with our findings on cell-cell interactions and Notch signaling in triggering oscillations. Because a fundamental feature of vertebrate axis elongation is the continuous flux of cells entering the PSM, excitability could provide competence to initiate oscillations and serve to synchronize cells with their neighbors.

Examples of excitable systems include neuron action potentials, heart Ca^{2+} waves, yeast glycolytic oscillations, and *Dictyostelium* cAMP oscillations (Mehta and Gregor, 2010). Excitability confers dynamical properties such as rapid synchronization, self-organization of traveling waves, existence of a threshold behavior tuning the competency of cells to signals, or specific responses to noise. While excitable properties have been previously discussed in the context of somitogenesis and the segmentation clock, this has never been directly tested experimentally (Cotterell et al., 2015; Masamizu et al., 2006; Tsiairis and Aulehla, 2016). Importantly, by accounting for the transition to an oscillatory state, we move beyond previous models that assumed intrinsic oscillations of isolated cells and thus focused on the phase dynamics of the oscillators (Oates et al., 2012). The more general framework of excitability also allows us to explain the formation of traveling waves in the absence of frequency gradients in our explants. More generally, our work shows how excitability might serve as a broad theoretical framework to understand vertebrate segmentation.

STAR★METHODS

Detailed methods are provided in the online version of this paper and include the following:

- KEY RESOURCES TABLE
- CONTACT FOR REAGENT AND RESOURCE SHARING
- EXPERIMENTAL MODEL AND SUBJECT DETAILS
  - Mice experiments
  - Chinese hamster ovary cell culture
  - Chicken experiments
- METHODS DETAILS
  - Explant cultures
  - Micropattern experiments
  - Immunohistochemistry
  - In situ hybridization
  - Probe preparation
  - Inhibitors treatments
  - qPCR
  - Lentivirus production and infection
  - Chicken electroporation
  - Simulations

SUPPLEMENTAL INFORMATION

Supplemental Information includes four figures, one table, ten movies, and one data file and can be found with this article online at http://dx.doi.org/10.1016/j.cell.2017.08.043.

AUTHOR CONTRIBUTIONS

A.H. designed, performed, and analyzed the biological and modeling experiments with O.P. L.M. interpreted experiments and observations in the context of excitable systems. I.R. contributed during the early stages of the project. A.H., L.M., and O.P. wrote the manuscript. OP supervised the project. All authors discussed and agreed on the results and commented on the manuscript.

ACKNOWLEDGMENTS

We thank members of the Pourquié lab, A. Aulehla, B. Bénazéraf, P. François, T. Gregor, D. Henrique, T. Hiscock, D. Ish-Horowicz, S. Megason, M. Oginuma, E. Özbudak, and S.D. Vincent for help and discussions. We thank S. Dupont, M. Elowitz, and Y. Saga for sharing reagents. Research in the Pourquié lab was funded by an advanced grant from the European Research Council, from the NIH (R01HD085121) and from the Human Frontier Science Program (RGP0051). A.H. was supported by fellowships from the French Ministry of Higher Education and Research and from the FRM (FDT20140930947). L.M. thanks the Schlumberger Foundation for partial financial support. L.M. was supported by a MacArthur Fellowship.

Received: December 19, 2016
Revised: June 23, 2017
Accepted: August 23, 2017
Published: September 21, 2017

REFERENCES

Allard, J., and Mogilner, A. (2013). Traveling waves in actin dynamics and cell motility. Curr. Opin. Cell Biol. *25*, 107–115.

Argentina, M., Coullet, P., and Mahadevan, L. (1997). Colliding waves in a model excitable medium: preservation, annihilation, and bifurcation. Phys. Rev. Lett. *79*, 2803–2806.

Aulehla, A., Wehrle, C., Brand-Saberi, B., Kemler, R., Gossler, A., Kanzler, B., and Herrmann, B.G. (2003). Wnt3a plays a major role in the segmentation clock controlling somitogenesis. Dev. Cell *4*, 395–406.

Aulehla, A., Wiegraebe, W., Baubet, V., Wahl, M.B., Deng, C., Taketo, M., Lewandoski, M., and Pourquié, O. (2008). A beta-catenin gradient links the clock and wavefront systems in mouse embryo segmentation. Nat. Cell Biol. *10*, 186–193.

Barrantes, I.B., Elia, A.J., Wünsch, K., Hrabe de Angelis, M.H., Mak, T.W., Rossant, J., Conlon, R.A., Gossler, A., and de la Pompa, J.L. (1999). Interaction between Notch signalling and Lunatic fringe during somite boundary formation in the mouse. Curr. Biol. *9*, 470–480.

Benazeraf, B., Francois, P., Baker, R.E., Denans, N., Little, C.D., and Pourquie, O. (2010). A random cell motility gradient downstream of FGF controls elongation of an amniote embryo. Nature *466*, 248–252.

Bessho, Y., Hirata, H., Masamizu, Y., and Kageyama, R. (2003). Periodic repression by the bHLH factor Hes7 is an essential mechanism for the somite segmentation clock. Genes Dev. *17*, 1451–1456.

Bone, R.A., Bailey, C.S.L., Wiedermann, G., Ferjentsik, Z., Appleton, P.L., Murray, P.J., Maroto, M., and Dale, J.K. (2014). Spatiotemporal oscillations of Notch1, Dll1 and NICD are coordinated across the mouse PSM. Development *141*, 4806–4816.

Chal, J., Oginuma, M., Al Tanoury, Z., Gobert, B., Sumara, O., Hick, A., Bousson, F., Zidouni, Y., Mursch, C., Moncuquet, P., et al. (2015). Differentiation of pluripotent stem cells to muscle fiber to model Duchenne muscular dystrophy. Nat. Biotechnol. *33*, 962–969.

Chapman, S.C., Collignon, J., Schoenwolf, G.C., and Lumsden, A. (2001). Improved method for chick whole-embryo culture using a filter paper carrier. Dev Dyn. *220*, 284–289.

Cooke, J., and Zeeman, E.C. (1976). A clock and wavefront model for control of the number of repeated structures during animal morphogenesis. J. Theor. Biol. *58*, 455–476.

Cotterell, J., Robert-Moreno, A., and Sharpe, J. (2015). A local, self-organizing reaction-diffusion model can explain somite patterning in embryos. Cell Syst. *1*, 257–269.

Dequéant, M.-L., Ahnert, S., Edelsbrunner, H., Fink, T.M., Glynn, E.F., Hattem, G., Kudlicki, A., Mileyko, Y., Morton, J., Mushegian, A.R., et al. (2008). Comparison of pattern detection methods in microarray time series of the segmentation clock. PLoS ONE *3*, e2856.

Duband, J.L., Dufour, S., Hatta, K., Takeichi, M., Edelman, G.M., and Thiery, J.P. (1987). Adhesion molecules during somitogenesis in the avian embryo. J. Cell Biol. *104*, 1361–1374.

Dubrulle, J., McGrew, M.J., and Pourquié, O. (2001). FGF signaling controls somite boundary position and regulates segmentation clock control of spatiotemporal Hox gene activation. Cell *106*, 219–232.

Dupont, S. (2015). Role of YAP/TAZ in cell-matrix adhesion-mediated signalling and mechanotransduction. Exp. Cell Res. *343*, 42–53.

Dupont, S., Morsut, L., Aragona, M., Enzo, E., Giulitti, S., Cordenonsi, M., Zanconato, F., Le Digabel, J., Forcato, M., Bicciato, S., et al. (2011). Role of YAP/TAZ in mechanotransduction. Nature *474*, 179–183.

Ferjentsik, Z., Hayashi, S., Dale, J.K., Bessho, Y., Herreman, A., De Strooper, B., del Monte, G., de la Pompa, J.L., and Maroto, M. (2009). Notch is a critical component of the mouse somitogenesis oscillator and is essential for the formation of the somites. PLoS Genet. *5*, e1000662.

Fitzhugh, R. (1961). Impulses and physiological states in theoretical models of nerve membrane. Biophys. J. *1*, 445–466.

Fuerer, C., and Nusse, R. (2010). Lentiviral vectors to probe and manipulate the Wnt signaling pathway. PLoS ONE *5*, e9370.

Gee, S.T., Milgram, S.L., Kramer, K.L., Conlon, F.L., and Moody, S.A. (2011). Yes-associated protein 65 (YAP) expands neural progenitors and regulates Pax3 expression in the neural plate border zone. PLoS ONE *6*, e20309.

Gelens, L., Huang, K.C., and Ferrell, J.E., Jr. (2015). How does the Xenopus laevis embryonic cell cycle avoid spatial chaos? Cell Rep. *12*, 892–900.

Gerber, A., Esnault, C., Aubert, G., Treisman, R., Pralong, F., and Schibler, U. (2013). Blood-borne circadian signal stimulates daily oscillations in actin dynamics and SRF activity. Cell *152*, 492–503.

Hansen, C.G., Moroishi, T., and Guan, K.-L. (2015). YAP and TAZ: a nexus for Hippo signaling and beyond. Trends Cell Biol. *25*, 499–513.

Harang, R., Bonnet, G., and Petzold, L.R. (2012). WAVOS: a MATLAB toolkit for wavelet analysis and visualization of oscillatory systems. BMC Res Notes *5*, 163.

Hirata, H., Yoshiura, S., Ohtsuka, T., Bessho, Y., Harada, T., Yoshikawa, K., and Kageyama, R. (2002). Oscillatory expression of the bHLH factor Hes1 regulated by a negative feedback loop. Science *298*, 840–843.

Hossain, Z., Ali, S.M., Ko, H.L., Xu, J., Ng, C.P., Guo, K., Qi, Z., Ponniah, S., Hong, W., and Hunziker, W. (2007). Glomerulocystic kidney disease in mice with a targeted inactivation of Wwtr1. Proc. Natl. Acad. Sci. USA *104*, 1631–1636.

Hu, J., Sun, S., Jiang, Q., Sun, S., Wang, W., Gui, Y., and Song, H. (2013). Yes-associated protein (yap) is required for early embryonic development in zebrafish (danio rerio). Int. J. Biol. Sci. *9*, 267–278.

Hubaud, A., and Pourquié, O. (2014). Signalling dynamics in vertebrate segmentation. Nat. Rev. Mol. Cell Biol. *15*, 709–721.

Izhikevich, E.M. (2000). Neural excitability, spiking and bursting. Int. J. Bifurcat. Chaos *10*, 1171–1266.

Kageyama, R., Ohtsuka, T., and Kobayashi, T. (2007). The Hes gene family: repressors and oscillators that orchestrate embryogenesis. Development *134*, 1243–1251.

Kamino, K., Fujimoto, K., and Sawai, S. (2011). Collective oscillations in developing cells: insights from simple systems. Dev. Growth Differ. *53*, 503–517.

Kim, N.-G., and Gumbiner, B.M. (2015). Adhesion to fibronectin regulates Hippo signaling via the FAK-Src-PI3K pathway. J. Cell Biol. *210*, 503–515.

Kim, W., Matsui, T., Yamao, M., Ishibashi, M., Tamada, K., Takumi, T., Kohno, K., Oba, S., Ishii, S., Sakumura, Y., and Bessho, Y. (2011). The period of the somite segmentation clock is sensitive to Notch activity. Mol. Biol. Cell *22*, 3541–3549.

Lauschke, V.M., Tsiairis, C.D., François, P., and Aulehla, A. (2013). Scaling of embryonic patterning based on phase-gradient encoding. Nature *493*, 101–105.

Levine, J.H., Lin, Y., and Elowitz, M.B. (2013). Functional roles of pulsing in genetic circuits. Science *342*, 1193–1200.

Lewis, J. (2003). Autoinhibition with transcriptional delay: a simple mechanism for the zebrafish somitogenesis oscillator. Curr. Biol. *13*, 1398–1408.

Liao, B.-K., Jörg, D.J., and Oates, A.C. (2016). Faster embryonic segmentation through elevated Delta-Notch signalling. Nat. Commun. *7*, 11861.

Manderfield, L.J., Aghajanian, H., Engleka, K.A., Lim, L.Y., Liu, F., Jain, R., Li, L., Olson, E.N., and Epstein, J.A. (2015). Hippo signaling is required for Notch-dependent smooth muscle differentiation of neural crest. Development *142*, 2962–2971.

Mara, A., and Holley, S.A. (2007). Oscillators and the emergence of tissue organization during zebrafish somitogenesis. Trends Cell Biol. *17*, 593–599.

Masamizu, Y., Ohtsuka, T., Takashima, Y., Nagahara, H., Takenaka, Y., Yoshikawa, K., Okamura, H., and Kageyama, R. (2006). Real-time imaging of the somite segmentation clock: revelation of unstable oscillators in the individual presomitic mesoderm cells. Proc. Natl. Acad. Sci. USA *103*, 1313–1318.

McGrew, M.J., Dale, J.K., Fraboulet, S., and Pourquie, O. (1998). The lunatic fringe gene is a target of the molecular clock linked to somite segregation in avian embryos. Curr Biol. *8*, 979–982.

Mehta, P., and Gregor, T. (2010). Approaching the molecular origins of collective dynamics in oscillating cell populations. Curr. Opin. Genet. Dev. *20*, 574–580.

Morales, A.V., Yasuda, Y., and Ish-Horowicz, D. (2002). Periodic Lunatic fringe expression is controlled during segmentation by a cyclic transcriptional enhancer responsive to notch signaling. Dev. Cell *3*, 63–74.

Morelli, L.G., Ares, S., Herrgen, L., Schröter, C., Jülicher, F., and Oates, A.C. (2009). Delayed coupling theory of vertebrate segmentation. HFSP J. *3*, 55–66.

Morin-Kensicki, E.M., Boone, B.N., Howell, M., Stonebraker, J.R., Teed, J., Alb, J.G., Magnuson, T.R., O'Neal, W., and Milgram, S.L. (2006). Defects in yolk sac vasculogenesis, chorioallantoic fusion, and embryonic axis elongation in mice with targeted disruption of Yap65. Mol. Cell. Biol. *26*, 77–87.

Murray, J.D. (2011). Mathematical Biology. II Spatial Models and Biomedical Applications (Springer).

Nagumo, J., Arimoto, S., and Yoshizawa, S. (1962). An active pulse transmission line simulating nerve axon. Proceedings of the IRE *50*, 2061–2070.

Naiche, L.A., Holder, N., and Lewandoski, M. (2011). FGF4 and FGF8 comprise the wavefront activity that controls somitogenesis. Proc. Natl. Acad. Sci. USA *108*, 4018–4023.

Nakao, H., Yanagita, T., and Kawamura, Y. (2014). Phase-reduction approach to synchronization of spatiotemporal rhythms in reaction-diffusion systems. Phys. Rev. X *4*, 021032.

Niwa, Y., Masamizu, Y., Liu, T., Nakayama, R., Deng, C.X., and Kageyama, R. (2007). The initiation and propagation of Hes7 oscillation are cooperatively regulated by Fgf and notch signaling in the somite segmentation clock. Dev. Cell *13*, 298–304.

Nowotschin, S., Ferrer-Vaquer, A., Concepcion, D., Papaioannou, V.E., and Hadjantonakis, A.K. (2012). Interaction of Wnt3a, Msgn1 and Tbx6 in neural versus paraxial mesoderm lineage commitment and paraxial mesoderm differentiation in the mouse embryo. Dev. Biol. *367*, 1–14.

Oates, A.C., Morelli, L.G., and Ares, S. (2012). Patterning embryos with oscillations: structure, function and dynamics of the vertebrate segmentation clock. Development *139*, 625–639.

Okubo, Y., Sugawara, T., Abe-Koduka, N., Kanno, J., Kimura, A., and Saga, Y. (2012). Lfng regulates the synchronized oscillation of the mouse segmentation clock via trans-repression of Notch signalling. Nat. Commun. *3*, 1141.

Ostrovsky, D., Cheney, C.M., Seitz, A.W., and Lash, J.W. (1983). Fibronectin distribution during somitogenesis in the chick embryo. Cell Differ. *13*, 217–223.

Palmeirim, I., Henrique, D., Ish-Horowicz, D., and Pourquié, O. (1997). Avian hairy gene expression identifies a molecular clock linked to vertebrate segmentation and somitogenesis. Cell *91*, 639–648.

Porazinski, S., Wang, H., Asaoka, Y., Behrndt, M., Miyamoto, T., Morita, H., Hata, S., Sasaki, T., Krens, S.F.G., Osada, Y., et al. (2015). YAP is essential for tissue tension to ensure vertebrate 3D body shape. Nature *521*, 217–221.

Pourquié, O., and Tam, P.P. (2001). A nomenclature for prospective somites and phases of cyclic gene expression in the presomitic mesoderm. Dev. Cell *1*, 619–620.

Preuße, K., Tveriakhina, L., Schuster-Gossler, K., Gaspar, C., Rosa, A.I., Henrique, D., Gossler, A., and Stauber, M. (2015). Context-dependent functional divergence of the Notch ligands DLL1 and DLL4 in vivo. PLoS Genet. *11*, e1005328.

Sawada, A., Shinya, M., Jiang, Y.J., Kawakami, A., Kuroiwa, A., and Takeda, H. (2001). Fgf/MAPK signalling is a crucial positional cue in somite boundary formation. Development *128*, 4873–4880.

Sgro, A.E., Schwab, D.J., Noorbakhsh, J., Mestler, T., Mehta, P., and Gregor, T. (2015). From intracellular signaling to population oscillations: bridging size- and time-scales in collective behavior. Mol. Syst. Biol. *11*, 779.

Shimojo, H., and Kageyama, R. (2016). Oscillatory control of Delta-like1 in somitogenesis and neurogenesis: A unified model for different oscillatory dynamics. Semin. Cell Dev. Biol. *49*, 76–82.

Sonnen, K.F., and Aulehla, A. (2014). Dynamic signal encoding–from cells to organisms. Semin. Cell Dev. Biol. *34*, 91–98.

Sprinzak, D., Lakhanpal, A., Lebon, L., Santat, L.A., Fontes, M.E., Anderson, G.A., Garcia-Ojalvo, J., and Elowitz, M.B. (2010). Cis-interactions between Notch and Delta generate mutually exclusive signalling states. Nature *465*, 86–90.

Tam, P.P.L., Meier, S., and Jacobson, A.G. (1982). Differentiation of the metameric pattern in the embryonic axis of the mouse. II. Somitomeric organization of the presomitic mesoderm. Differentiation *21*, 109–122.

Totaro, A., Castellan, M., Battilana, G., Zanconato, F., Azzolin, L., Giulitti, S., Cordenonsi, M., and Piccolo, S. (2017). YAP/TAZ link cell mechanics to Notch signalling to control epidermal stem cell fate. Nat. Commun. *8*, 15206.

Tsiairis, C.D., and Aulehla, A. (2016). Self-organization of embryonic genetic oscillators into spatiotemporal wave patterns. Cell *164*, 656–667.

Wahl, M.B., Deng, C., Lewandowski, M., and Pourquié, O. (2007). FGF signaling acts upstream of the NOTCH and WNT signaling pathways to control segmentation clock oscillations in mouse somitogenesis. Development *134*, 4033–4041.

Webb, A.B., Soroldoni, D., Oswald, A., Schindelin, J., and Oates, A.C. (2014). Generation of dispersed presomitic mesoderm cell cultures for imaging of the zebrafish segmentation clock in single cells. J. Vis. Exp. http://dx.doi.org/10.3791/50307.

Webb, A.B., Lengyel, I.M., Jörg, D.J., Valentin, G., Jülicher, F., Morelli, L.G., and Oates, A.C. (2016). Persistence, period and precision of autonomous cellular oscillators from the zebrafish segmentation clock. eLife *5*, e08438.

Winfree, A.T. (2001). The Geometry of Biological Time, Second Edition (New York: Springer).

Zhao, B., Li, L., Wang, L., Wang, C.-Y., Yu, J., and Guan, K.-L. (2012). Cell detachment activates the Hippo pathway via cytoskeleton reorganization to induce anoikis. Genes Dev. *26*, 54–68.

Please cite this article in press as: Hubaud et al., Excitable Dynamics and Yap-Dependent Mechanical Cues Drive the Segmentation Clock, Cell (2017), http://dx.doi.org/10.1016/j.cell.2017.08.043

STAR★METHODS

KEY RESOURCES TABLE

REAGENT or RESOURCE	SOURCE	IDENTIFIER
Antibodies		
Rabbit polyclonal anti-TBX6	Yumiko Saga lab	N/A
Mouse monoclonal anti-phospho-p44/42 MAPK (D13.14.4E)	CST	Cat#4370
Goat polyclonal anti-T	R&D	Cat#AF2085
Mouse monoclonal anti-YAP1	Santa-Cruz	Cat#63.7
Rabbit polyclonal anti-phospho YAP1 (Ser127)	Cell Signaling Technology	Cat #4911
Chicken polyclonal anti-GFP (detects Venus)	Abcam	Cat #13970
Chemicals, Peptides, and Recombinant Proteins		
Chir-99021	Sigma	Cat# SML1046
Mouse recombinant FGF4	R&D	Cat# 5846-F4
LDN-193189	Sigma/Stemgent	Cat# SML0559/Cat# 04-0074
BMS-493	Sigma	Cat#B6688
Heparin sodium salt from porcine intestinal mucosa	Sigma	Cat#H3393
Y-27632	P212121	Cat#LC-Y-5301
Y-27632 (for Figures 5E, 7H, 7I, and S3B)	Tocris	Cat#1254
Fibronectin	BD Biosciences	Cat# 356008
Mouse recombinant DLL1-Fc chimera	R&D	Cat#5026
DAPT	Sigma	Cat#D5942
LY-411575	Sigma	Cat# SML0506
Latrunculin A	Tocris	Cat# 3973
BSA	Thermo Fisher	Cat#15260037
Doxycyline	Sigma	Cat# D9891
Critical Commercial Assays		
SuperScript III First-Strand Synthesis System	Thermo Fisher	Cat#18080051
iTaq Universal SYBR Green Supermix	Biorad	Cat#1725121
Experimental Models: Cell Lines		
CHO – modified hN1 cell line	M.Elowitz lab (Sprinzak et al., 2010)	N/A
Experimental Models: Organisms/Strains		
LuVeLu	(Aulehla et al., 2008)	N/A
Fertilized White Leghorn chicken eggs	Charles River	10100330
Recombinant DNA		
Backbone of E[beta]C plasmid (BamHI/MluI)	(Fuerer and Nusse, 2010)	Addgene #24312
Sequence-Based Reagents		
qPCR primers – see Table S1	N/A	N/A
YAP5SA	S.Dupont (Dupont et al., 2011)	N/A
Hes7 intronic probe for *in situ* hybridization (first intron)	Kageyama lab (Bessho et al., 2003)	N/A
Msgn1 probe for *in situ* hybridization (entire coding region)	(Wahl et al., 2007)	N/A

(*Continued on next page*)

Continued

REAGENT or RESOURCE	SOURCE	IDENTIFIER
Sprouty2 probe for *in situ* hybridization	(Wahl et al., 2007)	N/A
Lfng probe for *in situ* hybridization	(McGrew et al., 1998)	N/A
Software and Algorithms		
MATLAB	MATLAB	MATLAB R2104
Prism	GraphPad	Prism 7.03
Other		
Zeiss LSM780 confocal microscope	Zeiss	N/A

CONTACT FOR REAGENT AND RESOURCE SHARING

Reagent requests should be directed and will be fulfilled by Olivier Pourquié (pourquie@genetics.med.harvard.edu).

EXPERIMENTAL MODEL AND SUBJECT DETAILS

All animal experiments were performed according to the institutions guidelines (IGBMC, France; Harvard Medical School/Brigham and Women's Hospital, USA).

Mice experiments

LuVeLu male mice were crossed with wild-type CD1 female mice (only *LuVeLu* males were used as it was more practical to sacrifice wild-type animals for colony maintenance reasons). Several genetic backgrounds were used without any noticeable effect on our experiments: 100% BL6 *LuVeLu*$^{+/-}$ males, 50%BL6;50%CD1 *LuVeLu*$^{+/-}$ males; 50%BL6;50%DBA/2 *LuVeLu*$^{+/-}$ males; 50% BL6;25%DBA/2;25%CD1 *LuVeLu*$^{+/+}$ males (for most of the experiments).

Chinese hamster ovary cell culture

CHO cells containing a synthetic reporter for Notch signaling (12xCSL-H2B::Citrine) and construct constitutively labeling nuclei (CMV-H2B::Cerulean) were a gift from M.Elowitz (Caltech) (modified version of the hN1 cell line (Sprinzak et al., 2010) with hNotch1 alone instead of a mCherry fusion). Cells were cultured in DMEM/F12 (Thermo Fisher #11320033) with 10%FBS in presence of L-Glutamine, Penicillin and Streptomycin. Cells were seeded on DLL1-coated dish (see above) and cultured overnight in presence of DAPT (25 μM), then medium was removed, cells were washed twice with culture medium without DAPT and cultured for one day before image acquisition on a EVOS Imaging station (Thermo Fisher). Latrunculin A was used at 0.5 μM.

Chicken experiments

Fertilized White Leghorn chicken eggs (Charles River) were incubated at 38°C to the desired stage.

METHODS DETAILS

Explant cultures

Embryos were collected at E9.5, and tails were then dissected out in DMEM with penicillin-streptomycin. Tails were then rinsed twice with PBS, rinsed once in Accutase (Life Technologies) and incubated in fresh Accutase at 37°C. After 7min30, tails were taken out of the incubator. Embryos were then rinsed once in DMEM, and incubated in dissection medium (DMEM 4.5g/L Glucose (Thermo Fisher #31053)), 15% FCS, 2mM L-Glutamine, 100U Penicillin, 100 μg/ml Streptomycin, 1x non-essential amino acid, HEPES 10mM – 0.22 μm-filtered). The tail bud mesenchyme was then isolated from the surrounding tissues (notably ectoderm) using a tungsten needle. Tail buds were then rinsed once in explant medium (dissection medium with 0.1mM of β-mercaptoethanol, Chir-99021 (Sigma) 3 μM, LDN-193189 (Sigma/Stemgent) 200nM, BMS-493 (Sigma) 2.5 μM, mFGF4 (R&D) 50ng/mL, heparin (Sigma) 1 μg/mL and Y-27632 (P212121/Tocris/Selleckchem) 10 μM) and transferred into culture dishes. Up to five explants were cultured in one well of a LabTek 8-well dish (450-500 μL) and positioned to avoid contact. Explants were incubated at 37°C, 7.5% CO2.

Explants were cultured on LabTek dishes coated with human plasma fibronectin: a solution of 4 μg/mL fibronectin in PBS was incubated for 2-3 hr at room temperature (250 μL for a well of a LabTek 8-wells dish). The dish was rinsed twice with PBS and incubated for at least 1h in dissection medium without HEPES. For experiments using the micropatterns, explants were cultured on 96-wells plate (tissue-culture treated) that was similarly coated with fibronectin; one explant was cultured per well in 100 μL before dissociation. For experiments with DLL1 coating, a 5 μg/mL solution of recombinant mouse DLL1-Fc chimera (R&D - #5026) was incubated for 2-3 hr at room temperature to coat the dish, then washed twice with PBS.

Micropattern experiments

For micropattern experiments, explants were cultured overnight, rinsed with PBS and dissociated with trypsin 0.05%-EDTA (18mM) at room temperature with gentle rocking. Explants were dissociated by pipetting up-and-down twice and collected in 1.5mL Eppendorf tubes. Cells were then spinned with an Eppendorf centrifuge 5430 (1810rpm/370rcf for 4min at room temperature). The supernatant was then aspired and cells were resuspended in 400 μL of explant medium by gently pipetting up-and-down the pellet. 100 μL of cell suspension was dispensed on a CYTOO 4-wells chamber with a CYTOOchip Arena coated with fibronectin. The chamber was let at room temperature for 10 min (without any movement to let the cells attach), then carefully transferred in a cell culture incubator at 37°C. After ~45 min, the medium was carefully aspired to remove floating cells and cells were rinsed once with 250 μL of dissection medium. Cells were then cultured with fresh explant medium (250 μL per well).

Immunohistochemistry

Explants were rinsed with PBS and fixed in fresh PBS, 4% PFA, then rinsed, washed three times in PBT (PBS, 0.1% Tween-20) and blocked with 10%FBS. Explants were then incubated overnight at 4°C with the following antibodies in PBT, 5% FBS: anti-TBX6 (gift from Yumiko Saga– 1:400), anti-phospho-p44/42 MAPK (Erk1/2)(Thr202/Tyr204) (D13.14.4E) (Cell Signaling Technology #4370 - 1:200), anti-T (R&D Systems - AF2085 –1:1000), anti-YAP1 (Santa Cruz 63.7 – 1:200), anti-phospho-YAP1 (Cell Signaling Technology – 1:200). Explants were then rinsed twice and washed six times for ~15 min at room temperature in PBT. Explants were blocked with PBT, 10% FBS and secondary antibodies coupled with Alexa fluorophores (Life technologies) were incubated overnight at 4°C or for 2 hr at room temperature, in PBT, 5% FBS. Nuclear staining was performed with Hoechst33342 (1:4000) and explants were mounted in Fluoromount G. For parasagittal sections, mice embryos were transferred in a series of PBS-sucrose solution after fixation, then embedded in OCT compound and frozen with liquid nitrogen. 20 μm sections were prepared using a Leica CM3050S cryostat and immunostaining was performed as previously described. All immunostaining data were acquired using a Zeiss LSM780 confocal microscope using a 20X (512x512 resolution) or 40X (1024x1024 resolution) (Figures 5B and S3B) objective.

In situ hybridization

Explants were fixed in fresh PBS, 4% PFA, and then rinsed, washed twice in PBT for 5 min. Samples were dehydrated in a sequence of PBT/MeOH (1:3, 1:1, 3:1), rinsed twice and incubated for ~30-60 min with pure cold methanol. Samples were rehydrated with a sequence of PBT/MeOH and washed three times with PBT for 5min. Explants were treated with proteinase K (1 μg/mL in PBT) for 5min, then rinsed with PBT and fixed with PBT, 4% formaldehyde, 0.2% glutaraldehyde for 20 min at room temperature. Samples were then washed twice in PBT, once in PBT/hybridization solution and twice in hybridization solution. The hybridization solution composition is 50% formamide, 5xSSC pH4.5, 1% SDS, 50 μg/mL yeast tRNA, 50 μg/mL heparin. Fresh hybridization solution was added and samples were incubated at 70°C for at least 2h. After this prehybridization, fresh hybridization solution with 500ng/mL of digoxigenin-labeled probes was heated at 70°C for ~10min and added to the samples for an overnight incubation at 70°C. Samples were rinsed twice and washed three times for 10-15 min with prewarmed Solution I (50% formamide, 5xSSC pH4.5, 1% SDS), and then rinsed once and washed three times for 10-15min with prewarmed Solution II (50% formamide, 2xSSC pH4.5, 0.11% Tween-20). Samples were cooled in Solution II at room temperature, rinsed twice and washed three times with TBT (TBS, 0.1% Tween-20). Explants were blocked twice using TBT, 20% Goat Serum, 2% Boehringer Mannheim blocking reagent. Antibody against digoxigenin coupled to alkaline-phosphatase (Roche) was incubated overnight at 4°C in blocking solution. Samples were rinsed twice and washed six times with TBT. Then, explants were rinsed twice and washed three times with NTMT (Tris pH 9.5 100 mM, NaCl 100 mM, $MgCl_2$ 50 mM, 0.1% Tween-20). Last, samples were rinsed once and incubated with BM Purple (Roche) at room temperature. For fluorescent *in situ* hybridization, an additional step with 3% H2O2 was performed after methanol dehydration. The anti-Digoxigenin-POD (poly), Fab fragments from Roche (11633716001) was used at 1:200 and the TSA Plus Cyanine 5 System kit was used with a dilution of 1:100 and an incubation time of 20 min. Pictures were taken on Leica M205FA. For chicken embryos, washes times were lengthened and 10 μg/mL of proteinase K for 12 min was used.

Probe preparation

In vitro transcription was performed on linearized plasmids or PCR products using the T3, T7 or Sp6 polymerases. DNA was then degraded using RQ1 DNase1 and RNA was precipitated using LiCl and ethanol. Probes were analyzed on agarose gel to confirm the purity and the size of the solution. The probes used were: mouse intronic *Hes7* (first intron), mouse *Msgn1* (coding sequence) (Wahl et al., 2007), mouse *Spry2* (Wahl et al., 2007), and chicken *LFNG* (McGrew et al., 1998).

Inhibitors treatments

To inhibit Notch signaling, explants were treated with DAPT (Sigma - 25 μM unless indicated), LY-411575 (Sigma - 10 μM unless indicated). To inhibit Yap signaling, explants were treated with latrunculin A (Tocris – 0.5 μM or 0.012 μM, 0.06 μM, 0.3 μM in Figure 7M)). Controls with vehicle solvent were used.

qPCR

RNA was extracted using Trizol (Life Technologies) according to the manufacturer's instructions. RNA concentrations were measured using a Nanodrop. Reverse transcription was performed with the same amount of total RNA using the Superscript III

kit (Life Technologies) according to the manufacturer's instructions (with a 1:1 mix of oligo-dT/random hexamers). Real-time PCR was performed on a Biorad CFX384 using iTaq Universal SYBR Green Supermix according to the manufacturer's instructions. For the real-time PCR, triplicates were performed and analyzed using the ΔΔCt method: i) Ct values were automatically retrieved from the CFX manager software (Biorad); ii) triplicates were averaged (if one sample was obviously different from the two others, it was excluded); iii) for each sample, the Ct for βactin was subtracted (ΔCt); iv) for each sample, the ΔCt of the reference sample was subtracted (ΔΔCt); v) the fold change was determined as $2^{-\Delta\Delta Ct}$. Standard deviations s_i for the Ct values were calculated, then standard deviations s_i^* for the ΔCt values were calculated as follows: $s_i^* = \sqrt{\left(\sqrt{s_i^2 + s_{housekeeping}^2}\right)}$; the range for fold change was determined as $2^{-\Delta\Delta Ct \pm si*}$.

Primers were validated by checking that the melting curve had a single defined peak and by validating the efficiency of amplification using serial dilution (between −3.6 and −3.2). Sequences are presented in Table S1.

Lentivirus production and infection

The YAP5SA construct was amplified from a plasmid containing the FLAG-hYAP-5SA (gift from S.Dupont) and cloned into the E[beta]C plasmid (Addgene#24312) cut with BamHI and MluI. An empty control was prepared using only the backbone of the E[beta]C (cut BamHI and self-ligated). Lentivirus was produced in 293T cells: cells were transfected using the $CaCl_2$ method with the packaging plasmids psPAX2 (Addgene #12260) and pVSVG (gift from M.Wernig lab). Supernatant was collected, filtered using a 0.45 μM filter and concentrated by centrifugating 4 volumes of supernatant on 1 volume of TNE buffer (50mM Tris pH7.2, 100mM NaCl, 0.5mM EDTA, 15% sucrose) at 7197 rcf for 4 hr at 4°C. Explants were infected for ∼4 hr and further incubated overnight before starting a movie. Infected cells were detected thanks to the *SV40-mCherry* reporter of the E[beta]C backbone.

Chicken electroporation

We dissected chicken embryos at stage HH5-7 and electroporated them by injecting a DNA solution (7.5 μg/ μL of pBI-mCherry-Yap5SA; 1.5 μg/ μL of pCAGGS-rtTA-m2; 0.6 μg/ μL of pCAGGS-Venus) in the space between the vitelline membrane and the epiblast surrounding the anterior primitive streak level, which contains the precursors of the paraxial mesoderm. The pBI-mCherry-Yap5SA plasmid is a bidirectional vector leading to the expression of mCherry and YAP5SA upon doxycyline expression and rtTA-M2 presence; pCAGGS-Venus was used as a control for electroporation. *Ex ovo* electroporations were carried out with five successive square pulses of 8V for 50ms, keeping 4mm distance between anode and cathode using Petri dish type electrodes (CUY701P2, Nepa Gene, Japan) and a CUY21 electroporator (Nepa Gene, Japan). Embryos were then cultured using the EC culture system (Chapman et al., 2001). After 10-12 hr of incubation, embryos were checked for correct development and electroporation using the fluorescence of the pCAGGS-Venus vector. Then, 100 μL of PBS with or without doxycycline (10 μg/ mL – Sigma D9891) was added under and above the embryo and embryos were further incubated for 11-14 hr before fixing them. To double-check that electroporated embryos treated with PBS only were correctly electroporated, we performed an immunostaining for Venus after the *in situ* hybridization using standard methods ((Benazeraf et al., 2010) – chicken polyclonal antibody Abcam #13970).

Simulations

Simulations were performed using the FitzHugh-Nagumo model. This model was formulated by Fitzhugh (1961) and Nagumo et al. (1962) to simulate the electrical activity of neurons. It comprises two variables, an activator (here designed as *u*), and a repressor (here designed as *v*).

The differential equations describing the temporal evolution of the substances *u* and *v* are:

$$\tau_u \frac{du}{dt} = u.(u-a)(1-u) - v + I + \varepsilon$$

$$\tau_v \frac{dv}{dt} = u - g.v$$

Where:

- τ_u and τ_v are the timescale dynamics of *u* and *v*; typically, for an excitable system, $\tau_u << \tau_v$ meaning that the changes in activator amount occurs much faster than for the inhibitor;
- **a** is the excitability threshold. When the system is in a steady state, it is the minimal quantity of activator required to excite the system and generate a pulse;
- I is an external stimulus provided to the system that induces the production of activator;
- ϵ is a noise term that reflects the stochasticity of the different reactions;
- g is a degradation term for the repressor

In this model, the activator rapidly induces the repressor and itself, while the repressor inhibits the activator. The existence of a fast positive feedback and a slow negative feedback is frequent in excitable systems.

These equations can display three types of dynamics: *i)* the system is at a steady state and fluctuates around its equilibrium because of noise or small stimuli; *ii)* the system displays a pulsatile behavior, as it transiently crosses the excitability threshold following a strong stimulus; *iii)* the system is permanently above the excitability threshold and shows stable oscillations (limit-cycle oscillator). In the latter case, the FitzHugh-Nagumo model is similar to other models of phase-coupled oscillators (Nakao et al., 2014).

To illustrate the dynamical behavior of excitable systems, we can consider the electrical activity of neurons. The activator *u* corresponds to the membrane potential of the neuron, while the repressor *v* is a "recovery" variable that indicates the inactivation of ion channels. The excitability threshold a would correspond to the membrane potential above which action potentials are generated, while the stimulus I would refer to the electrical current imposed by electrodes in a patch-clamp setting. In this system, the rapid opening of voltage-sensitive channels forms a fast positive feedback, while their inactivation reflects the slow negative feedback ($\tau_u << \tau_v$). Therefore, the system is rapidly excited and then channels cannot be excited again because of this slow negative feedback; such state is refered to as a refractory period and is a common feature of excitable systems. Below the excitability threshold, a small stimulus causes only a transient depolarization of the membrane, while a strong stimulus can provoke an action potential. When this stimulus is constant, the neurons display regular oscillations. Alternatively, when the excitability threshold is lowered, neurons can be in a self-oscillatory mode (e.g., pacemakers neurons), as only the cellular noise is sufficient to generate action potentials. In our case, we model the dynamics of a single-cell and postulate that Yap signaling sets the excitability threshold a, while Notch signaling is modeled using the variable I.

Importantly, the FitzHugh-Nagumo model does not make any assumption about the actual molecular details of the system, but can accurately predict its dynamical behavior without knowledge of the ions channels nature and properties. That is, the complex molecular interactions can be reduced to an activator-repressor couple and still capture the dynamics of the system. Therefore, the FitzHugh-Nagumo model has been widely used to describe the behavior of various excitable systems, such as the cAMP oscillations in social amoeba (Sgro et al., 2015), calcium oscillations in *Xenopus* (Gelens et al., 2015) or the polymerization of actin (Allard and Mogilner, 2013).

Simulations were performed using MATLAB R2104. Behavior of the activator and repressor was simulated using the differential equations of Figure 7 using the Runge-Kutta method. The following parameters were used: $\tau_u = 0.25$, $\tau_v = 30$, $g = 0.25$. For the noise, we used a white noise and a colored noise to mimic stochastic and large fluctuations in cells (similarly to Webb et al., 2016). We simulated the Notch inhibition by a decrease in I (I = 1 to I = 0), and the LatA treatment as a decrease in a (a = 0.4 for explants, a = 0.2 for partial rescue of oscillations with LatA, and a = −0.4 for full rescue with LatA, a = 0.6 for dissociated cells, a = 0.9 for caYAP). The strength of the noise was increased in dissociated cells as suggested by the experimental profiles of dissociated cells. To simulate the experiments with increasing concentration of LatA, we varied the excitability threshold to 0.45, 0.3, 0.15, 0. Twenty cells were simulated and the number of pulses was manually counted. A version of the code is presented in Data S1 in the case of an untreated explant.

QUANTIFICATIONS AND STATISTICAL ANALYSIS

Image analysis

Quantification of LuVeLu fluorescence in explants

Kymographs were done in Fiji by drawing a rectangle from the starting center of the traveling waves to the edge of the explant perpendicular to the direction of the wave. The intensity along the long axis was measured and the image was smoothened (this filter replaces each pixel with the average of its 3 × 3 neighborhood).

Fluorescence intensity profiles were done by selecting a circular region of interest in Fiji and by measuring the total intensity over time for this region; *LuVeLu* intensity is given in arbitrary units (normalized by the initial value) and a smoothing function (average over three points) was applied.

Quantification of pERK signal

For the quantification of nuclear staining and pERK intensity, a rectangular region of interest was drawn (as shown in Figure 1) and analyzed using MATLAB: the region (830 μm in length) was divided in 20 boxes along the center-periphery axis; the fluorescence intensity signal was measured within each box, and then normalized by the minimal value of the series.

Quantification of LuVeLu fluorescence in single-cell

For single-cell tracking, we manually tracked cells that have no/few contacts with other cells. For cells on fibronectin, a contour was manually drawn using Fiji for each time point; for latrunculin A treated cells a circle of constant area was drawn for all time-points. We obtained the raw mean fluorescence of the *LuVeLu* reporter and subtracted the mean background fluorescence of a region near the cells; we then normalized all data by dividing to their first value. Fluorescence intensity shows the mean fluorescence smoothed by applying a moving average over five points (with equal weight). To obtain the "instantaneous" intensity, we subtracted the mean fluorescence averaged over 150 min to the mean fluorescence at each point, and then applied a smoothing over five points. Fast Fourier analysis was performed and plotted with MATLAB using the *fft* function.

Quantification of LuVeLu fluorescence in micropatterns

For the quantification of micropattern experiments, a region of interest encompassing the entire surface of one circle (80 μm diameter for Figure 3B, 225 μm diameter otherwise) was drawn and the *LuVeLu* intensity was measured using the Time Series Analyzer V3 plugin on Fiji. The period in Figure 2A was measured by measuring the time between two peaks or two troughs. The average intensity was measured by averaging the intensity over 3 hr to avoid instantaneous variations dues to the oscillations.

Determination of LuVeLu amplitude

For the quantification of the amplitude of oscillations before DAPT removal, we used the difference between the maximum and minimum values of *LuVeLu* fluorescence during the first 150 min of the movie to define the ''amplitude'' at time 0. After DAPT removal, amplitude was manually calculated as the difference between the *LuVeLu* intensities at the peak and trough of oscillations. For the quantification of the amplitude of oscillations after DAPT addition in single cells, we only measured the difference of intensities between the peak and the next trough as the curve has an asymmetric shape.

Determination of LuVeLu oscillations phase

To extract the phases of *LuVeLu* oscillations in single cells in explants treated with latrunculin A, we measured the raw fluorescence intensity of single cells and used the WAVOS toolkit (Harang et al., 2012) using Gaussian edge correction and removing edge-affected data.

Quantification of the YAP1 nucleocytoplasmic ratio

For the quantification of the nucleocytoplasmic ratio of YAP1 intensity, we used MATLAB to automatically measure the intensities of YAP1 in the nucleus and in the cytoplasm and compare it to the overall level of nuclear staining in the image (as a proxy for cell density).

Statistics

For the measurement of the period between the center and the periphery, four explants were used and the period was measured as the time between two troughs. This gave 33 measurements for each condition (center versus periphery), a two-tailed (equal variance) t test was performed using Excel. For the analysis of the correlation between the nucleocytoplasmic ratio of Yap and the nuclear staining intensity per pattern, we performed a linear correlation analysis using the function corr() on MATLAB.

For the analysis of the differences in number of pulses with different doses of latrunculin a, we performed a one-way ANOVA test followed by Sidak's multiple comparisons test using GraphPad Prism7.

DATA AND SOFTWARE AVAILABILITY

The code for the simulations is available in Data S1.

Cell

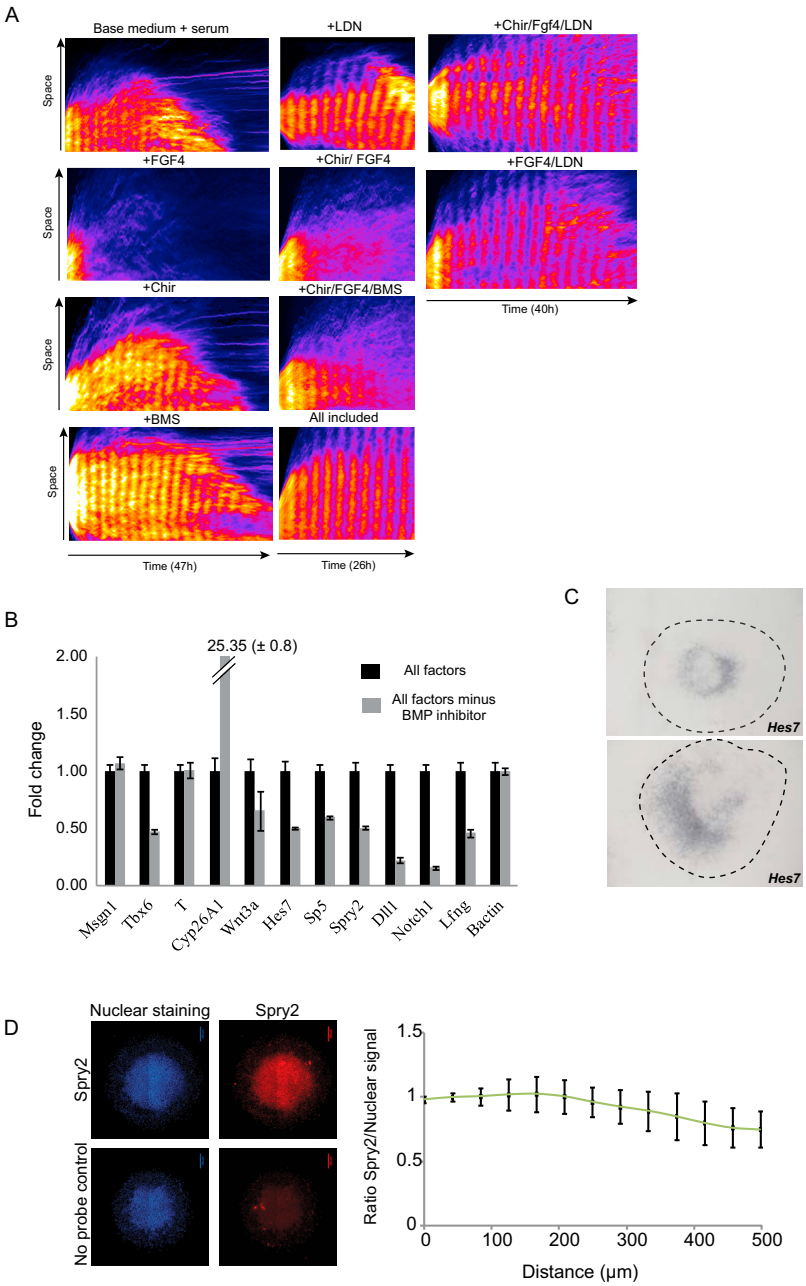

Figure S1. Establishment of an *In Vitro* System to Study *LuVeLu* Oscillations, Related to Figure 1

(A) Kymographs showing the effects of different growth factors activators or inhibitors on the dynamics of *LuVeLu* oscillations. Base medium consists of DMEM, 15%FBS, L-Glutamine, Non-Essential Amino Acids, Penicillin, Streptomycin, β-mercaptoethanol, HEPES and Rock inhibitor. Addition of Chir (n = 3/3), BMS (n = 3/3), LDN (n = 3/3) or FGF4/LDN (n = 2/2) did not prevent the arrest of oscillations and differentiation after one day of culture. Addition of FGF4 led to a decrease in the *LuVeLu* intensity and the loss of oscillations (n = 4/5). Similar phenotype was obtained after combined addition of Chir and FGF4 (n = 5/5). Addition of the BMP inhibitor LDN to Chir and FGF4 led to the apparition of sustained oscillations, even if sporadic differentiation was observed in absence of the retinoic acid inhibitor BMS (n = 1/1). Addition of BMS along with Chir and FGF4 led to dampened oscillations (n = 2/3).

(B) Graph showing the fold change in gene expression (± SD) for explants cultured for one day in control conditions (black) or in Chir/FGF4 (gray). 4 explants were pooled per condition.

(C) *In situ* hybridization for the cyclic gene *Hes7* using an intronic probe. Dashed lines represent the edges of explants.

(D) (Left) *In situ* hybridization for the Fgf target *Sprouty2* and nuclear staining. (Right). Quantification of the ratio of fluorescence between Sprouty2 signal and nuclear signal (± SD) from the center to the periphery of the explants.

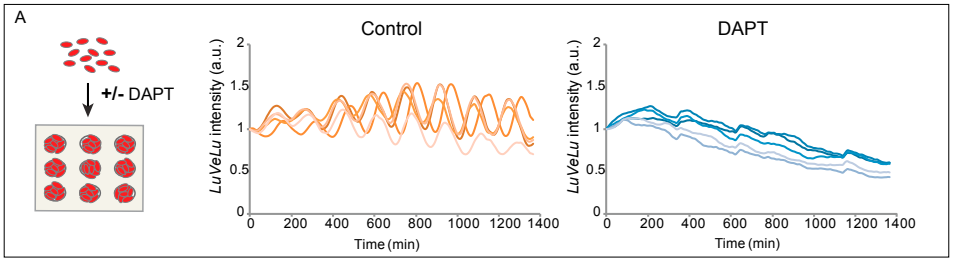

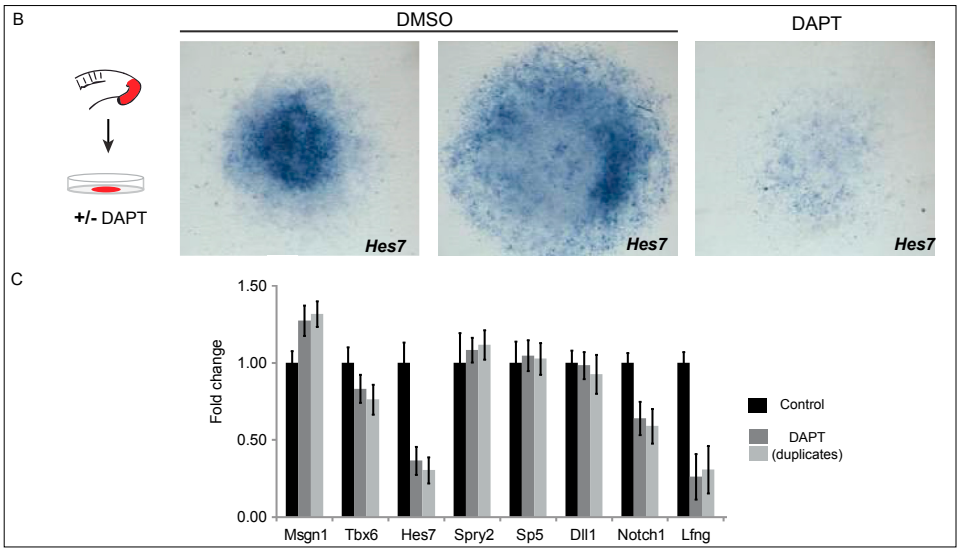

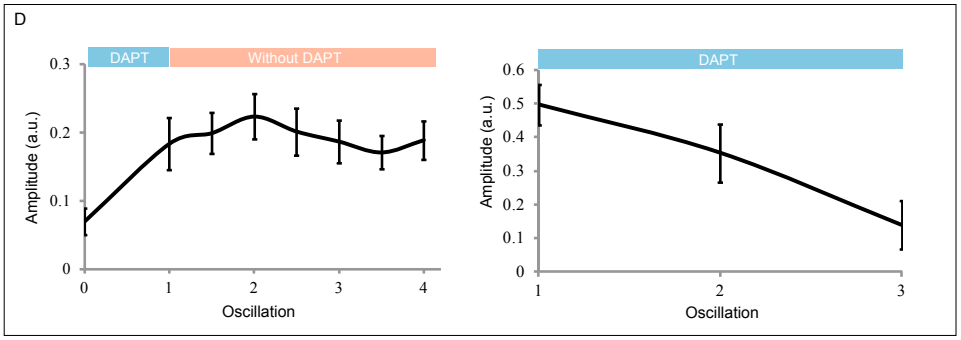

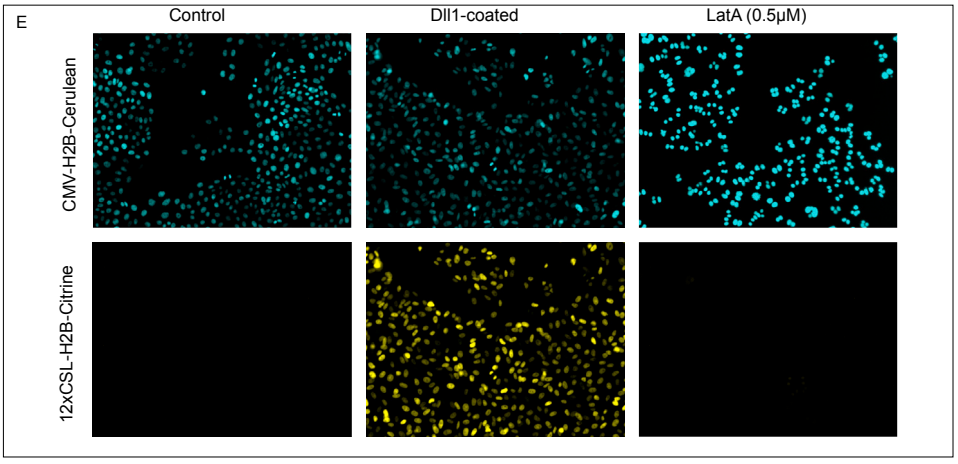

(legend on next page)

Figure S2. Notch Signaling Regulates *LuVeLu* and *Hes7* Oscillations, Related to Figure 4

(A) Graphs showing the intensity of the fluorescent reporter *LuVeLu* over time for cells on micropattern treated with vehicle control or DAPT (20 μM) after seeding. Each line corresponds to one entire pattern.

(B) *In situ* hybridization for the cyclic gene *Hes7* using an intronic probe. (Left) Explants treated with vehicle control. (Right) Explant after an overnight treatment with DAPT (20 μM) showing a strong decrease in staining (n = 3/3).

(C) Graph showing the fold changes in gene expression (± SD) for explants cultured for one day, and then treated for 6 hr with DMSO or DAPT (20 μM) (biological replicates). One sample represents 3 explants pooled.

(D) Graphs showing the amplitude (± SD) of *LuVeLu* oscillations over time after DAPT removal (left) or addition (right).

(E) Notch reporter activity in CHO cells containing a synthetic reporter (bottom – *12xCSL-H2B::Citrine*) and a nuclear marker (top – *CMV-H2B::Cerulean*) for cells on control tissue culture-treated dish (left), for cells on tissue culture-treated dish coated with DLL1 (middle), and for cells on tissue culture-treated dish with LatA (right).

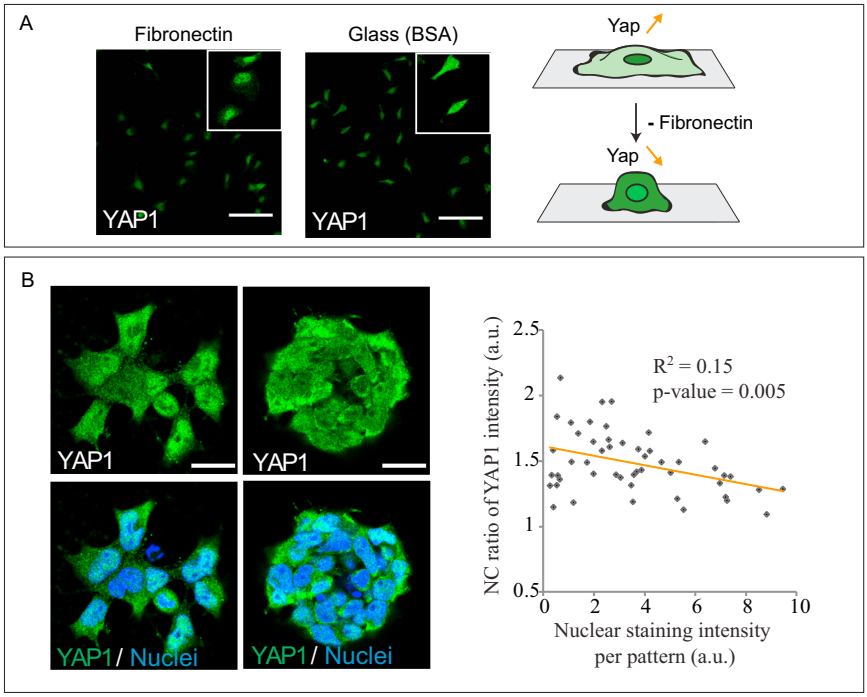

Figure S3. Onset of *LuVeLu* Oscillations Is Controlled by the Adhesion Substrate, Related to Figure 5

(A) (Left) Immunostaining for YAP1 in isolated cells cultured on a substrate coated with fibronectin or BSA. (Right) Scheme of the changes in nucleo-cytoplasmic localization of YAP1 upon changes in cell adhesion.

(B) (Left) Immunostaining for YAP1 in PSM cells at low (left) and high (right) density on fibronectin micropattern (scale bar, 20 μm). (Right) Graph showing the nucleo-cytoplasmic (NC) ratio of YAP1 as a function of the intensity of nuclear staining.

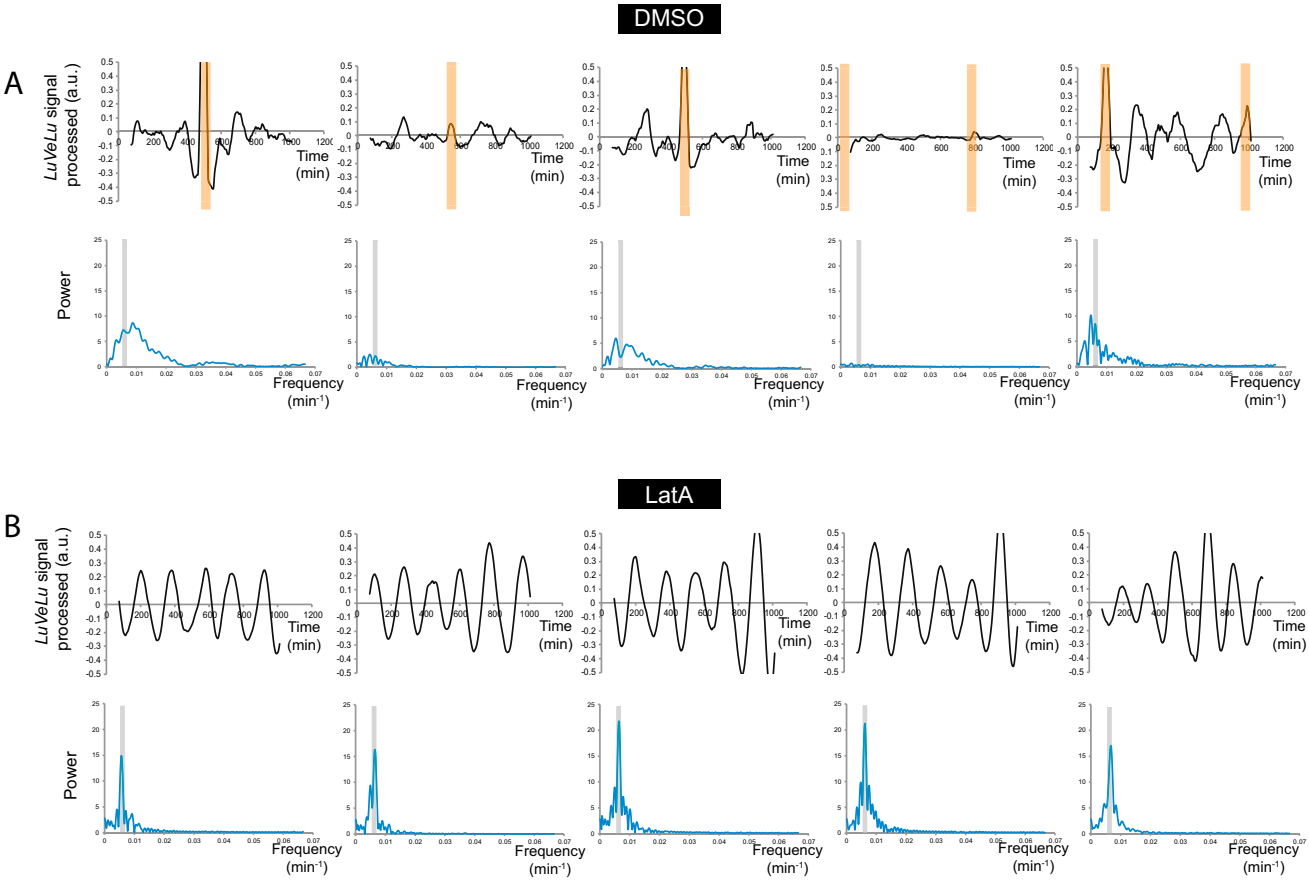

Figure S4. Latrunculin A Treatment Can Trigger *LuVeLu* Oscillations in Single Cells, Related to Figure 5

(A). Graphs showing the intensity of the fluorescent reporter *LuVeLu* over time for dissociated cells cultured on a fibronectin substrate after subtraction of the average fluorescence (see the STAR Methods). Orange boxes indicate cell divisions. The associated power spectrum from Fourier analysis is represented (the gray area represents period in the range of 150-175 min).

(B) Graphs showing the intensity of the fluorescent reporter *LuVeLu* over time for dissociated cells cultured on a fibronectin substrate and treated with LatA after subtraction of the average fluorescence (see the STAR Methods). Orange boxes indicate cell divisions. The associated power spectrum from Fourier analysis is represented (the gray area represents period in the range of 150-175 min).